Kinetic modelling of biomass fast devolatilization using Py-MS: Model-free and model-based approaches

Manel NASFi, Marion Carrier, Sylvain Salvador

Kinetic modelling of biomass fast devolatilization using Py-MS: Model-free and model-based approaches

Manel Nasfi, Marion Carrier, Sylvain Salvador

RAPSODEE, CNRS UMR 5203, Université de Toulouse, IMT Mines Albi, Campus Jarlard, 81013 Albi CT Cedex 09, France

A B S T R A C T

Feasibility using quantitative data obtained from a micropyrolyzer coupled to an evolved gas analysis technique, mass spectrometry, for kinetics determination has been long demonstrated. This paper describes for the first time how to obtain intrinsic kinetics for fast devolatilization of biomass and its lignocellulosic fractions (e.i., hol-ocellulose and lignins). The main challenge with online detection is assessing the time lag related to transport phenomena between the reactor and the detector. To do this, an experimental method was developed to derive the real-time biomass devolatilization profile; this provided 'corrected' datasets. Preliminary kinetic parameters were obtained from the differential isoconversional Friedman method combined with real-time sample tem-perature history. Not considering the effect of thermal lag and the delay in detecting pyrolysis products by the MS leads to a certain level of inaccuracies. Isoconversional activation energy (E_α) dependencies obtained in the absence of heat and mass transfer limitations for biomass and its components highly varied with conversion, confirming the multi-step nature of the fast pyrolysis process. After demonstrating the modeling limitations of a constant activation energy model (CAEM), both isoconversional functions were parametrized to propose a variable activation energy model (VAEM) and used as initial inputs for the distributed activation energy model.

1. Introduction

Fast pyrolysis is one of the most efficient thermochemical technologies to transform biomass into a renewable energy resource [1]. Biomass is rapidly heated without oxygen, producing vapors, aerosols, char, and non-condensable gases. Vapors and aerosols are condensed into a dark brown liquid called pyrolytic oil or bio-oil, which can be easily stored and transported [2]. The increasing and significant potential of pyrolytic oil for producing energy, fuels, commodity, and high-value chemicals [3] depends on research breakthroughs in process modeling and bio-oil upgrading technologies [4–6]. Bio-oil yields and composition depend on reactor configuration, operating conditions, and the nature of biomass [7]. Considering the wide variety in the chemical composition of lignocellulosic biomasses and reactor types, it is unsurprising that controlling pyrolysis product yields and composition remains challenging [8].

The absence of suitable experimental methods and techniques is the main problem in determining fast pyrolysis kinetics and reaction chemistry [9]. The thermogravimetric analyzer (TGA) is the most common equipment for studying pyrolysis kinetics. TGA gives information about the whole process without providing qualitative information on pyrolysis products related to mass loss. A strategy of coupling TGA with Fourier transform infrared (FT-IR) spectroscopy and mass spectrometry (MS) has been proposed to overcome this disadvantage [11–15]. However, the typical heating rates of TGA (0.01–1.66 °C/s) are unsuitable for studying fast pyrolysis [14,15].

The Frontier micropyrolyzer allows equivalent heating of biomass particles to that of a fluidized bed reactor, reaching a maximum temperature ramp of 110 °C/s for the cup containing the biomass sample [16]. The inability to directly monitor the reaction temperature of the sample has been overcome with the last findings of our group [16]. We have demonstrated that under certain sample preparation and heating and gas flow conditions, dynamic pyrolysis experiments with isothermal reacting samples could be conducted knowing the temperature-time profile, which is essential for kinetic evaluation.

In addition, measuring the reaction kinetics of solid particles requires efficiently measuring the time-resolved composition of evolving product species. When using offline analysis mode, pyrolysis reactors must have milliseconds time scales to track the progress of the reaction even at earlier stages. For example, the particular design of the PHASR reactor

or wire mesh reactor facilitates the collection of primary volatiles via rapid separation and quenching that minimizes secondary reactions [17,18]; biomass pyrolysis in these reactors can be precisely controlled to stop the reaction in milliseconds. Alternatively, online analysis techniques can be used to follow the dynamics of the formation of volatiles and measure reaction kinetics. However, it takes time (kiloseconds) for instruments like gas chromatographic systems (GC or GC-MS) to separate the complex mixtures, making online studies difficult [17]. Online mass spectrometry analysis has the advantages of high sensitivity and high-speed acquisition (up to ms per spectrum) [19]. The evolved gas analysis has recently been applied, directly coupling the analytical pyrolyzer to mass spectrometry [20,21]. However, it has been performed using slow heating rates. The increasing progress in online mass spectrometry applications exhibits its advantage in exploring the dynamics of volatile formation during the pyrolysis process, which is hardly achieved by offline analytical methods [19]. The time delay in species detection and molecular diffusion are generally present in the online detection technique [17]. In this study, particular efforts have been made to quantify the extent of molecular diffusion and advection within the reactor and transfer line before reaching the detector.

A detailed mechanistic model can ideally predict the fast pyrolysis of biomass [10]. However, developing a rigorous mechanistic model remains challenging [22]. Most models expanding the thermal decomposition of biomass can be considered pseudo-mechanistic, for which assumptions about the underlying chemistry are required, but their kinetic parameters fit experimental data [23]. Devolatilization reactions are commonly described as chemical components (cellulose, hemicelluloses, and lignins) or pseudo-components. These summative models are based on the assumption that the devolatilization of each component proceeds independently. Component reactions can be combined in parallel, serial, or complex schemes. More advanced models increase the number of components to improve the accuracy of the predictions. Selecting a kinetic model that reasonably represents the pyrolysis process without too many parameters is essential to prevent overfitting. Other approaches in solid fuel devolatilization consider using distributed activation energy (DAEM). In this case, varying the activation energy simulates a series of independent and parallel reactions. The distribution function can take different forms. The Gaussian distribution has been successfully used for the thermal decomposition of coals and later adapted to biomasses [24]. Model selection is a critical step in the model-fitting approach. The selected model needs to balance simplicity and goodness of fit. Various reaction models exist for the solid-state kinetic evaluation, and they can be categorized into three major types: accelerating, decelerating, and sigmoidal. Among these, the first-order reaction model, which falls under the decelerating type, is commonly used to represent the biomass decomposition process. It offers a simple representation where the rate is highest at the beginning and decreases continuously as the extent of conversion increases. However, a sigmoidal model, such as the Avrami–Erofeev models, is often more appropriate for the pyrolysis of cellulose-based materials [25]. The sigmoidal model captures the characteristic behavior observed in cellulose decomposition, where the initial reaction rate increases, reaches a maximum and decreases as the process proceeds. This model provides a more accurate representation of the complex kinetics involved in biomass pyrolysis.

Several recent studies have promoted the use of isoconversional methods to assess the chemical reactivity (e.g., with the determination of isoconversional activation energy) of a complex chemical process without assuming any form for the reaction model [15,26–29]. Meaningful mechanistic insights can be drawn from those trends [29,30]. Yet, the overall prediction of the biomass pyrolysis process requires an explicit mathematical form for both intertwined chemical and physical phenomena [31].

This paper explicitly describes overcoming kinetics inaccuracies when using a conventional micropyrolyzer system by developing novel calibration strategies for the Py-MS system to consider the effect of thermal lag and the delay in the detection of pyrolysis products by the MS. The most common differential isoconversional method applied to corrected Py-MS data was then used to interpret and model primary mechanisms of biomass devolatilization. Both constant and variable activation energy models were developed based on the results of the isoconversional method to simulate fast biomass devolatilization, and outcomes were compared to those of the distributed activation energy model.

2. Materials and methods

2.1. Feedstock materials and characterization

Zea Mays leaves (IsoLife, Wageningen, Netherlands) and Beechwood (SoWood, Saint-Herblain, France) were used in this study. The size of samples was reduced to < 100 μm using cryogenic grinding (SPEX 6775 model). Before analysis, biomass samples were dried for 24 h at 104 °C. Proximate analysis based on the ASTM E1131 standard using TGA/DSC 111 Setaram and ultimate analysis using an elemental analyzer (Flash 2000 Thermo) were performed, and the results are presented in Table A.1 in Supplementary material, section A.

The lignocellulosic composition (e.i., the weight percentage of cellulose, hemicelluloses, and lignins) of feedstocks (Table A.1 in Supplementary material, section A) was estimated using the thermogravimetric method proposed by Carrier et al. [32]. Lignins and holocellulose contents were also measured experimentally based on ISO 21436 and ISO 21437 standard methods for the beechwood sample (values between brackets in Table A.1 in Supplementary material, section A). The cellulose, hemicelluloses, and lignins contents obtained with this method were comparable to others in literature for beechwood (cellulose: 40–50 wt%, hemicelluloses: 24–40 wt%, and lignins: 18–25 wt%) [33,34] and corn stover (cellulose: 20–40 wt%, hemicelluloses: 23–46 wt%, and lignins: 16–26 wt%) [33,34]. Beechwood sample contains high volatile matter content, which generally contributes to high bio-oil yields, while *Zea Mays* leaves with high fixed carbon may lead to high biochar yield [34]. *Zea Mays* leaves show higher content of ash than beechwood. The inorganic biomass sample fraction mainly consists of potassium and calcium (Table A.2 in Supplementary material, section A).

2.2. Methods

2.2.1. Data acquisition

Raw devolatilization profiles were acquired through analytical pyrolysis experiments performed in a multi-shot pyrolyzer (EGA/PY-3030D) coupled with a mass spectrometer (Agilent 5977), as shown in Fig. 1.a. In the pyrolyzer, the "single-shot" mode was used. The pyrolysis unit (Fig. 1.b) consists of a sampler that holds samples, the reactor made in Quartz, a heating sleeve, ceramic support, an insulator, and a heated interface zone to keep the pyrolysis products in the gaseous state until they reach the GC injection port. The micro-furnace is preheated from ambient temperature to the desired pyrolysis temperature (400, 420, 430, and 450 °C) in less than one second [35]. The furnace was calibrated before experiment to ensure accuracy.

Approximately 50 μg of biomass sample was carefully introduced to the deactivated stainless-steel cup to spread out as well as possible at the bottom of the cup and get as close as possible to the thin film configuration to ensure a kinetically controlled regime [16]. The sample holder allows the introduction of the cup containing the biomass sample into the center of the microreactor by releasing the stick once the micro-furnace is preheated. Before introducing the sample, the microreactor was purged for 2 min to remove oxygen. Pyrolytic products were conducted using Helium (Scientific grade 6.0, Linde France) at a flow rate of 100 mL/min. They left the microreactor through a needle attached to the bottom of the interface zone, which directs them to the transfer line. Temperatures of the interface zone and the GC injection port were set to 280 °C. The transfer line consists of a deactivated metal

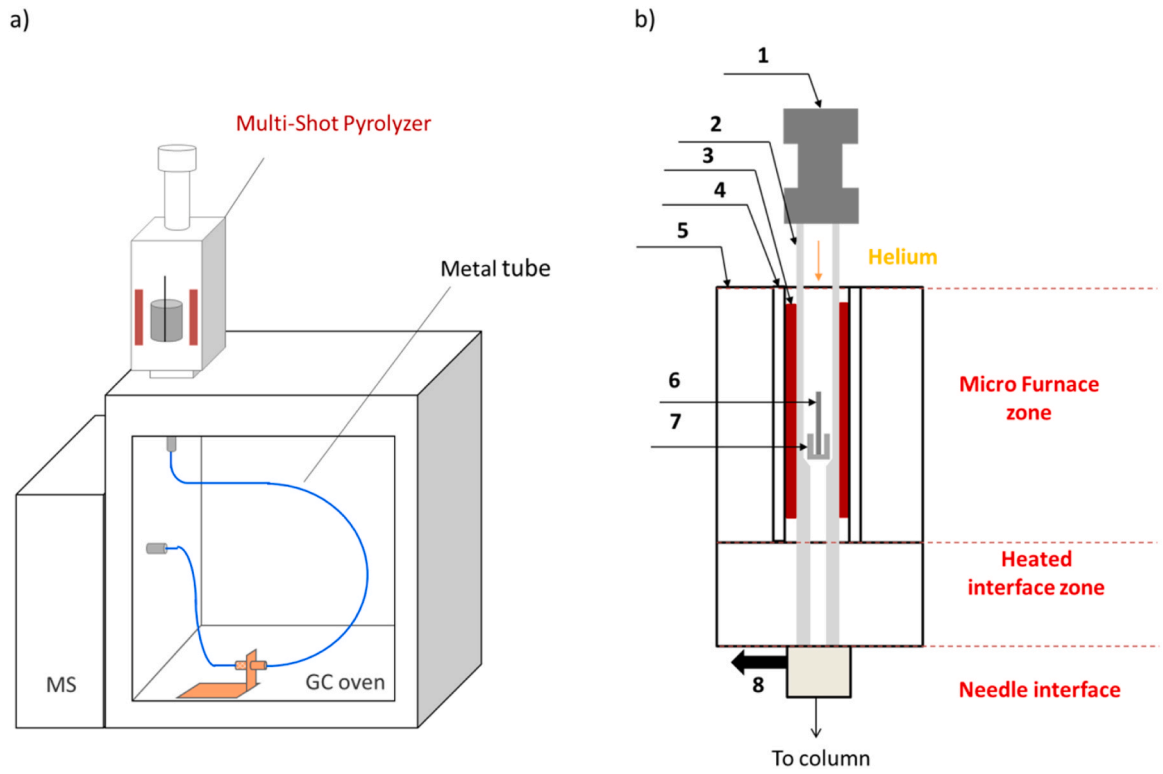

Fig. 1. a) System configuration of the Py-MS analysis. b) Schematic description of the pyrolyzer. 1: sampler, 2: reactor (Quartz tube), 3: heating sleeve, 4: ceramic support, 5: insulator, 6: stick, 7: cup, and 8: split vent.

tube (UADTM-2.5 N, 2.5 m lenght; 0.15 mm i.d.) that connects the injector and the MS detector, kept at 300 °C. A primary limitation of the experimental setup is the discrimination of detecting high molecular weight compounds with higher-boiling points due to the constraint of the GC injection port that cannot exceed 300 °C [36]. The released products were injected using a split ratio of 100:1, so only 1.0 mL/min of carrier gas flow rate crosses the deactivated column. The mass spectrometer was operated under electron impact mode at an ionization energy of 70 eV, scanning from 32 to 300 m/z.

To investigate the contribution of biomass biopolymers, the main representative fragments of holocellulose and lignins (Table B.1 in Supplementary material, section B) were extracted from the devolatilization profiles using the OpenChrom® data analysis system. These signals were selected based on their relative intensities and because they are markers of the corresponding components of biomass.

As temperature errors can affect kinetic prediction [37], this study uses temperature-time histories, T(t), of biomass samples obtained using a thermal model developed in our previous work [16], where the detailed procedure is described. T(t) profiles of biomass sample for each furnace temperature are displayed in Fig. 2 and confirm the non-isothermal character of a heating period of fewer than 6 s. These T (t) profiles will be incorporated into the kinetic calculation.

Finally, cumulative Residence Time Distribution (RTD) measurements were carried out. Indeed, molecular and convective transport phenomena compromise the collection of intrinsic kinetic data [17]. A deconvolution technique is required to obtain real-time devolatilization profiles to clear the intrinsic kinetic data from bias. Cumulative residence time distribution, F(t), is obtained from a step injection of gas mixture (10 mol.% of propene, 10 mol.% of butene-1, 10 mol.% of cis-butene-2, and 10 mol.% of *trans*-butene-2 in azote) at a flow rate of 2 mL/min). The syringe driver pushed the gas mixture through a PTFE tube (Fig. 3). The end of the tube was connected to a long needle, which was inserted into the reactor allowing the gas mixture to be injected at the cup location. The mass spectrometer recorded tracer signals at the same experimental conditions as acquiring the devolatilization profiles. Two tracer injections for each set of experimental conditions ensure reproducibility testing.

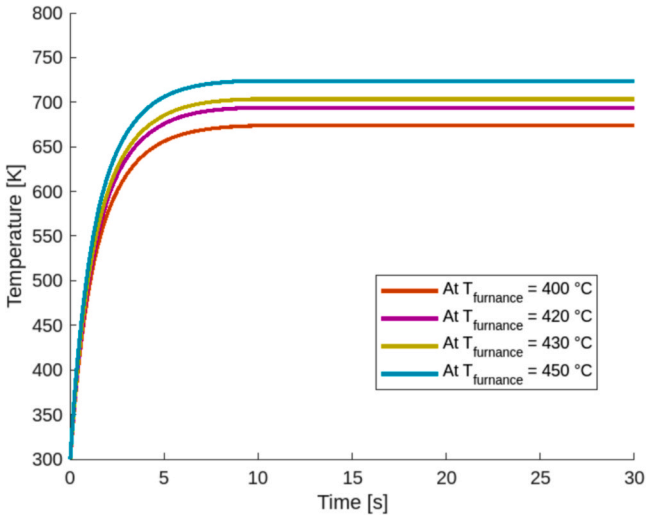

Fig. 2. Temperature histories of biomass samples at the different furnace temperatures.

2.2.2. *Data processing*

Raw devolatilization and cumulative residence time profiles were processed using Matlab R2022a software. Firstly, raw devolatilization signals were divided by the initial mass of samples. Signal fluctuations shown in Fig. C.1 in Supplementary material, section C were minimized by smoothing the raw devolatilization using the classic Savitzky and Golay methods. Then signal curves with baseline correction were

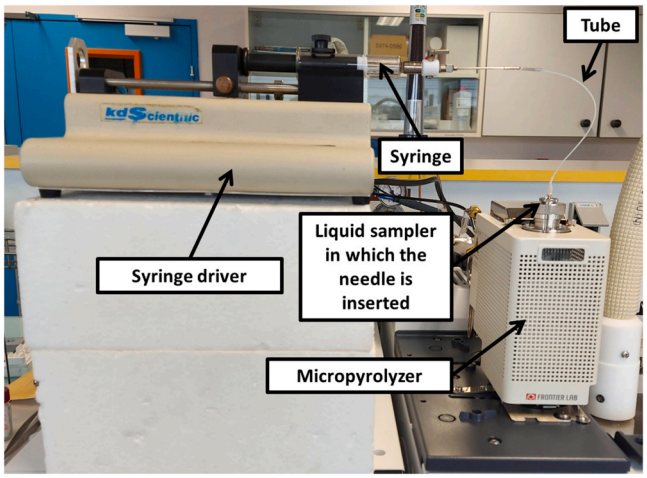

Fig. 3. Residence Time Distribution measurement setup.

constructed and normalized to the maximum intensity (Fig. C.2 in Supplementary material, section C).

Tracer signals were recorded following the negative step injection (Fig. D.1 in Supplementary material, section D). The response to this negative step injection constitutes the raw cumulative residence time distribution curves, F(t). The positive step injection response was used to deal with noises of negative step responses as described in Supplementary material, section D. F(t) curves were then baseline-corrected and normalized to the maximum intensity (Fig. D.3 in Supplementary material, section D). The slight variation in F(t) curves when varying furnace temperature indicates that the characteristic time of molecules transport inside the deactivated column is more significant than that inside the microreactor as the temperature change occurs only inside the reactor while the deactivated column temperature remains constant for all experiments. RTD curves, E(t), were obtained by differentiating F(t) to time and were normalized to the total area so that $\int_0^{+\infty} E(t)dt = 1$ [38].

2.2.3. Real-time devolatilization profile determination

Researchers commonly utilize procedures based on deconvolution mathematical operations to correct the time lag between product evolution and product detection in the evolved gas analysis [37,39,40]. It is important to note that this technique differs from peak resolution, also known as peak deconvolution, which separates and resolves overlapping peaks in chromatographic separation. The underlying mathematics of these two techniques are distinct.

The principle of the used technique for this study is that the observed profile can be described as a convolution of the real-time devolatilization profile, g(τ), with the system response function, E(τ) [39]:

$$(g * E)(t) = \int_{-\infty}^{+\infty} g(\tau)E(t-\tau)d\tau \tag{1}$$

Thus, the deconvolution operation aims to reverse the effects of this convolution and retrieve the real-time devolatilization profile. Two methods can be employed to achieve this. The first method involves Fourier transforming the data and dividing it by the system response function (E(t)). This approach allows for removing the system response function from the detected profile. Alternatively, the second method involves using an objective function that compares the measured data to the convolution of the instrument response function and the trial kinetics function, which is used in the various versions of the KINETICS software.

By utilizing either of these methods, researchers can effectively correct the time lag and recover the real-time devolatilization profile in evolved gas analysis. This study used Fast Fourier Transform (FFT) to obtain the real-time devolatilization profile from the couple Residence time distribution (RTD)-raw devolatilization profile. FFT requires a high number of data points to ensure a satisfactory frequency resolution [41]. Thus, RTD and raw devolatilization profiles were zero-padded before FFT calculation. As deconvolution "is an improper mathematical operation, very sensitive to noise in the raw signals" [42], a further filtering action has been implemented. Thus, an iterative filtering method was performed as described by Liliedahl et al. [43]. Finally, the filtered devolatilization profiles were multiplied to the maximum value (intensity/initial sample weight) to obtain the same unit as the raw devolatilization profiles. The Matlab code for the deconvolution process is presented in Supplementary material, section E.

The comparison between the detected and real-time responses (Fig. 4) shows that the deconvoluted devolatilization profiles for biomass samples were offset in front, with slight changes in the "shape" (i.e., including the high, the width, and the tailing behavior principally). The advection is the main process responsible for shifting peaks because of species transit inside the system. However, profile shape differences may result from the contribution of dispersion and molecular diffusion inside the transfer line. The "shoulder" at the back of the devolatilization peak for beechwood became more apparent after the deconvolution process (Fig. 4.b, curve AA). It should also be noted that this "shoulder" is hardly recognizable in the raw devolatilization profile (Fig. 4.b, curve A), confirming the need to correct the devolatilization profiles to understand the kinetics of pyrolysis properly.

2.2.4. Kinetic analysis

Traditionally, the kinetic rate of biomass decompositions is based on the following equation [22]:

$$\frac{d\alpha}{dt} = k(T)f(\alpha) \tag{2}$$

where t (s) is the time, T (K) is the temperature, α is the extent of conversion, f(α) is the reactional model, and k(T) is the rate constant usually expressed by the Arrhenius law:

$$k(T) = A\exp\left(-\frac{E}{RT}\right) \tag{3}$$

where A (s^{-1}) is the pre-exponential factor, E ($J.mol^{-1}$) is the activation energy, and R ($J.mol^{-1}. K^{-1}$) is the gas constant.

For Py-MS data, the calculation of reactional conversion is based on measurements of ion intensity, I_t, in Ampere, which, once integrated over the pyrolysis time and multiplied by both molecular weight of volatile species, MW, and flow rate, $\dot{V}$, results in the released mass during the reaction:

$$\alpha = \frac{\int_0^t I_t \quad MW \quad \dot{V}dt}{\int_0^{\infty} I_t \quad MW \quad \dot{V}dt} = \frac{A_t}{A_{tot}} \tag{4}$$

The extent of conversion for integral data (e.g., TGA, DMA, capacity data) is calculated using Eq. (5) [30], whereas, for Py-MS data, it is computed as the case of differential data (e.g., DSC) using Eq. (6) [30].

$$\alpha = \frac{X_t - X_{t_0}}{X_f - X_t} \tag{5}$$

$$\alpha = \frac{X_t}{X_{tot}} \tag{6}$$

where X is a physical property that is associated with the process transformation. In our case, X_t and X_{tot} in Eq. (6) are, respectively, the real-time total ion chromatogram area between 0 and t, A_t, and the entire area of the real-time devolatilization profile, A_{tot} (Eq. 4).

2.2.4.1. Isoconversional method. When applying the isoconversional kinetic methodology, the isoconversional principle is invoked (i.e., "the

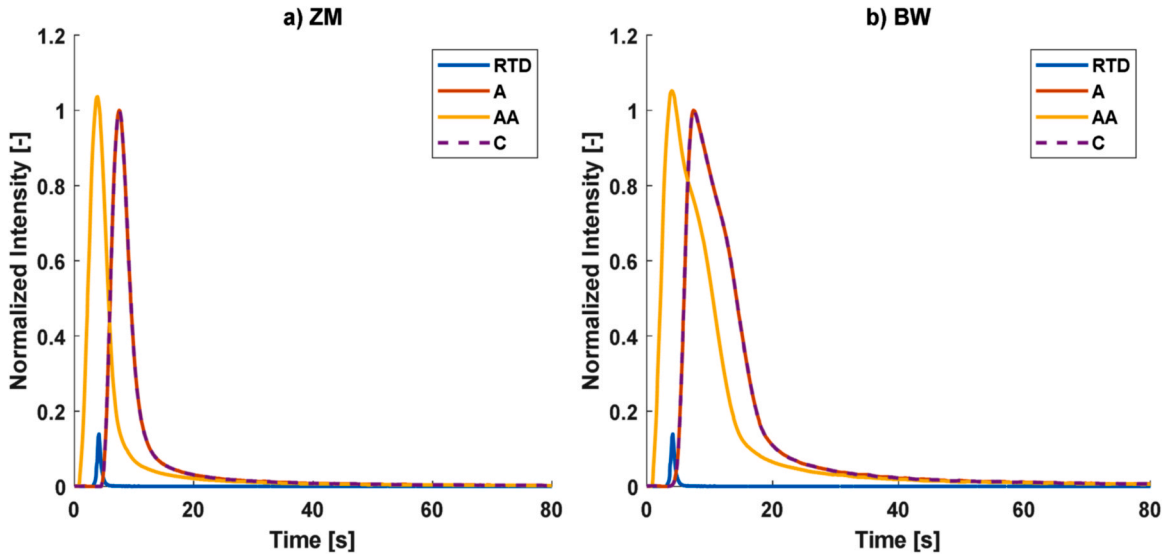

Fig. 4. Deconvolution process for determining the real-time devolatilization profiles of *Zea Mays* leaves (a) and beechwood (b) at $T_{furnace} = 450\ ^{\circ}C$. RTD is the residence time distribution curve, A is the raw devolatilization profile, AA is the deconvoluted profile, and C is the convolution test.

process rate at the constant extent of conversion is only a function of temperature") and specific recommendations made by ICTAC [29] (e.g., use the extent conversion range of 0.05–0.95 and experiences at different temperature programs) must be applied. The differential Friedman isoconversional method, described by Eq. (7), was used in this study.

$$\ln\left(\frac{d\alpha}{dt}\right)_{\alpha,i} = \ln(A_\alpha f(\alpha)) - \frac{E_\alpha}{RT_{\alpha,i}} \tag{7}$$

where *i* is the index corresponding to each temperature history, E_α, and $\ln(A_\alpha f(\alpha))$ are the isoconversional values of both effective activation energy and pre-exponential factor. The Friedman method assumes that the chemistry of the process is independent of T on a narrow temperature interval and only dependent on the extent of conversion, α. And it is through the plots of $\ln\left(\frac{d\alpha}{dt}\right)_{\alpha,i}$ versus 1/T that E_α and $\ln(A_\alpha f(\alpha))$ can be determined without the assumption of the reactional model.

Numerical differentiation of the conversion data using the finite difference method was carried out to obtain the derivative conversion data, dα/dt [27]:

$$\left(\frac{d\alpha}{dt}\right)_i = \begin{cases} \dfrac{\alpha_{i+1}-\alpha_i}{t_{i+1}-t_i} \; for \quad start \quad point \\ \dfrac{1}{2}\dfrac{\alpha_i-\alpha_{i-1}}{t_i-t_{i-1}} + \dfrac{1}{2}\dfrac{\alpha_{i+1}-\alpha_i}{t_{i+1}-t_i} \; for \quad intermediate \quad points \\ \dfrac{\alpha_i-\alpha_{i-1}}{t_i-t_{i-1}} \; for \quad end \quad point \end{cases} \tag{8}$$

For applying the Friedman analysis (Eq. 7), $(\ln(d\alpha/dt))_{\alpha,i}$, and T_α need to be determined. These values were estimated based on α(t), T(t), and (dα/dt)-t curves using the cubic spline interpolation, ensuring accurate continuity between data points. E_α/R and $\ln(A_\alpha f(\alpha))$ were determined by linear regression based on two datasets for each temperature history. The regression coefficient, R^2, was also estimated. Finally, confidence intervals based on standard deviations were determined for E_α.

The isoconversional method was applied for real-time devolatilization profiles and by integrating the temperature history of samples, which is one of the original aspects of this study, as most similar studies considered a constant heating rate [20,44].

The same isoconversional analysis was applied to raw devolatilization profiles and considering isothermal profiles (in this case, "*i*" in Eq. (7) represents the constant furnace set temperature) to evaluate the impact of transport phenomena on modifying devolatilization kinetics. Friedman diagrams, $(\ln(d\alpha/dt)_{(\alpha,i)}$ versus 1/T, can be found in Supplementary material, section F for each case: isothermal and non-isothermal conditions with raw devolatilization profiles (Figs. F.1 and F.2) and non-isothermal and real-time devolatilization profiles using the fully corrected kinetic datasets (Fig. F.3).

2.2.4.2. Variable activation energy model (VAEM). For this study, an empirical model with variable kinetic parameters developed by Gábor Várhegyi [45] was applied to model the complex devolatilization of biomass and its main components. This model is based on the combination of Eqs. (2 and 3) while approximating E_α and $A_\alpha \times f(\alpha)$ by relatively simple mathematical formulas (Eq. 9). Eq. (10) is a rearrangement of Eq. (9) where the term (1 - α) does not reflect the assumption of the first-order model, but it ensures that dα/dt would be 0 at α = 1. This model, therefore, keeps the principle of being "model-free." A new parameter is introduced here, $\tilde{A}_\alpha$, and is equal to $A_\alpha \times f(\alpha) / (1 - \alpha)$ when $\alpha < 1$. The division by (1 - α) is not possible when α is equal to 1, so $\tilde{A}_\alpha$ may have any finite value there.

$$\frac{d\alpha}{dt} = \widetilde{A_\alpha}(1-\alpha) \quad \exp\left(\frac{-E_\alpha}{RT(t)}\right) \tag{9}$$

Taking the logarithm of $\tilde{A}_\alpha$ and rearranging Eq. (9) leads to the following:

$$\frac{d\alpha}{dt} = (1-\alpha) \quad \exp\left(\ln\left(\widetilde{A_\alpha}\right) - \frac{E_\alpha}{RT(t)}\right) \tag{10}$$

Polynomials approximate $\ln(\tilde{A}_\alpha)$ and E_α to obtain flexible approximations with limited numbers of unknowns. For this purpose, the variable x equal to $2 \times \alpha - 1$ is introduced, which varies from − 1 to + 1 as α varies from 0 to 1. Thus, E_α and $\ln(\tilde{A}_\alpha)$ were fifth-order polynomials described by the variable x:

$$E_\alpha = a_0 + a_1x + a_2x^2 + a_3x^3 + a_4x^4 + a_5x^5 \tag{11}$$

$$\ln(\widetilde{A_\alpha}) = b_0 + b_1x + bx^2 + b_3x^3 + b_4x^4 + b_5x^5 \tag{12}$$

The unknown parameters of the model were obtained based on the least squares method by minimizing the difference between the observed rate, $(d\alpha/dt)^{obs}$, and their counterparts calculated from the given model, $(d\alpha/dt)^{calc}$, as described by the following objective function:

$$OF = \sum_{j=1}^{N_{exp.}} \sum_{i=1}^{N_j} \frac{\left(\left(\frac{d\alpha}{dt}\right)_j^{obs}(t_i) - \left(\frac{d\alpha}{dt}\right)_j^{calc}(t_i) \right)^2}{N_j \quad h_j^2} \tag{13}$$

In this case, the objective function minimizes the difference considering all the experimental tests performed at different temperature programs presented by $N_{exp.}$. N_j is the number of points for each j experiment, and h_j is the maximum observed rate of the given experiment. The division by the highest observed rate is helpful to counterbalance the magnitude differences [46].

The 'quasi-newton' algorithm in Matlab® coupled with the 'fminunc' function for unconstrained problems was built to determine the optimal parameters that can minimize the objective function (Eq. 13). Finally, the fit quality for the eight experiments, $reldev_8$, corresponding to duplicate for four heating programs, is the mean root square of relative deviations, determined for each experiment by the following equation:

$$reldev_i(\%) = 100 \left\{ \sum_{j=1}^{N_j} \frac{\left(\left(\frac{d\alpha}{dt}\right)_j^{obs}(t_i) - \left(\frac{d\alpha}{dt}\right)_j^{calc} \quad (t_i) \right)^2}{N_j \quad h_j^2} \right\}^{0.5} \tag{14}$$

2.2.4.3. Distributed activation energy model (DAEM). The distributed activation energy model (DAEM) is used to fit experimental results and to be compared to the variable activation energy model (VAEM). It is a multiple-reaction model representing the pyrolysis process through a large number of independent and parallel reactions characterized by their own activation energy and pre-exponential factor. In this study, we used the 1st-order DAEM. The derivation of the 1st-order DAEM to obtain the final equation (Eq. 15) is presented in Supplementary material, section G.1.

$$\frac{d\alpha}{dt} = \int_0^{\infty} A\exp\left[-\frac{E}{R \quad T(t)} - \int_0^t A\exp\left(-\frac{E}{R \quad T(t)} \right) dt \right] D(E)dE \tag{15}$$

In this equation, α is the extent of conversion, t (s) is the time, A (s^{-1}) is the pre-exponential factor, E_i (J/mol) is the apparent activation energy, R ($J.mol^{-1}.\ K^{-1}$) is the gas constant, and T (K) is the absolute temperature. It is further assumed that all reactions share the same frequency factor, so the reactivity distribution is represented by a continuous distribution of activation energies, $D(E)$ (mol/J). The Gaussian distribution (Eq. 16) centered at E_0 (J/mol) with standard deviation σ (J/mol), widely used for biomass pyrolysis, is chosen for this work. This study also performs a comparative analysis of predicted results using one- and double-Gaussian DAEM.

$$D(E) = \frac{1}{\sigma\sqrt{2\pi}} \quad \exp\left[-\frac{(E - E_0)^2}{2\sigma^2} \right] \tag{16}$$

The double-Gaussian DAEM is introduced in this study to present the reactivity distribution of holocellulose and lignin so:

$$D(E) = c_1 \quad D_1(\mathrm{E}) + c_2 \quad D_2(\mathrm{E}) \tag{17}$$

where $D_1(E)$ and $D_2(E)$ are Gaussian distributions, and c_1 and c_2 are the weight parameters or the corresponding contributions of holocellulose and lignins devolatilization.

The sample temperature profile is taken into consideration for this model. Thus, the DAEM is treated for a non-isothermal case. Calculating kinetic parameters requires iterative loops of double integral functions, leading to significant numerical complications [24]. This work evaluates the DAEM equation by the Gauss-Hermite integration, as described in Supplementary material, section G.2.

Optimal parameters (A, E_0, and σ for 1 G-DAEM and A_1, A_2, E_{01}, E_{02}, σ_1, σ_2, c_1, and c_2 for 2 G-DAEM) are obtained by minimizing the objective function (Eq. 13) in the same way as described earlier.

3. Results and discussions

3.1. Devolatilization profiles of biomass fast pyrolysis

The comparison of real-time devolatilization profiles versus time obtained at several furnace temperatures for beechwood (BW) and *Zea Mays* leaves (ZM) (Fig. 5) reveals a significant difference in thermal behavior between woody and grassy materials already reported [47]. These results denote a pyrolysis time of ~30 s at 400 °C, decreasing to ~15 s at 450 °C for the complete devolatilization of ZM, whereas BW devolatilization is almost twice longer than that of ZM devolatilization with a pyrolysis time of ~50 s at 400 °C and ~25 s at 450 °C. At higher temperatures, the maximum devolatilization of two biomasses is reached during the heating period, confirming that conversion achieved during this stage should be considered. The faster the reaction, the more conversion takes place during sample heating. The time evolution of volatile matter release is generally linked to the lignin content [48]. Indeed, the devolatilization of BW takes longer than that of ZM due to its higher lignin content of 24.5 wt% against 19.4 wt% for ZM (Table A.1 in supplementary material, section A). The presence of ash, which is about 7.5 wt% for ZM, higher than that of BW, 0.3 wt%, can also catalyze/inhibit pyrolysis reactions [49,50]. The detection of higher intensity obtained for the pyrolysis of ZM (Fig. 5) confirms a more consequent release of low molecular weight compounds, which is undoubtedly related to the different nature of lignins [51] and the most significant inorganic content within straw materials [52,53].

Thermal conversion curves (Fig. 6) show that more than 30% of biomass was converted before reaching the set temperature of 450 °C. This confirms that an isothermal experiment cannot be claimed using this experimental equipment and the necessity of considering the sample temperature history when studying fast pyrolysis kinetics. The initial induction period, characterized by a low decomposition rate (Fig. 6), can be attributed to the sample heat-up process and also to the contribution from the sigmoidal reaction characteristics of specific biomass components. However, in our case, where the experiment exhibits a non-isothermal behavior for a significant period, it becomes challenging to identify the sigmoidal characteristic of biomass decomposition. Recognizing the sigmoidal characteristic is more straightforward in isothermal data because the rate constant, k(T), remains constant (Eq. 2). Therefore, the shape of the kinetic curve is solely determined by the reaction model itself. However, under non-isothermal conditions, both the rate constant (k(T)) and the reaction model (f(α)) vary simultaneously, resulting in sigmoidal α vs. t curves. This simultaneous variation makes it more challenging to recognize the specific reaction model type.

The data collection for this study is done under a kinetic-controlled regime as verified by the same authors in a previous study [16] and confirmed by investigating the sample weight effect on thermal conversion inherent to MS spectra measured by Py-MS (see Supplementary material, section H).

Py-MS spectra (with a mass-based fraction collection between m/z 32–300) of ZM and BW devolatilization obtained at different furnace temperatures were time-averaged (Supplementary material, section I). Non-significant changes between average spectra collected at 400, 420, 430, and 450 °C for both types of biomass indicate the absence of new low and polar molecular weight compounds that could eventually highlight a drastic change in the pyrolysis chemistry. An example of Py-MS spectra obtained at $T_{furnace}$ = 430 °C is shown in Fig. 7 and reveals the slight effect of the biomass nature in modifying the type and the distribution of the analyzed species. This variation is generally linked to the amount of cellulose, hemicelluloses, and lignins in the biomass [54,55]. Both spectra show a significant peak at m/z 43, the acylium ion originating from the electron ionization of carbonyl compounds [56].

The prominent peak at m/z 43 is typical of the pyrolysis of biomass containing alkali materials [56,57]. Alkali metals, including potassium and sodium, one of the most abundant inorganics in biomass, are known to change the kinetics of carbohydrates primary decomposition and their

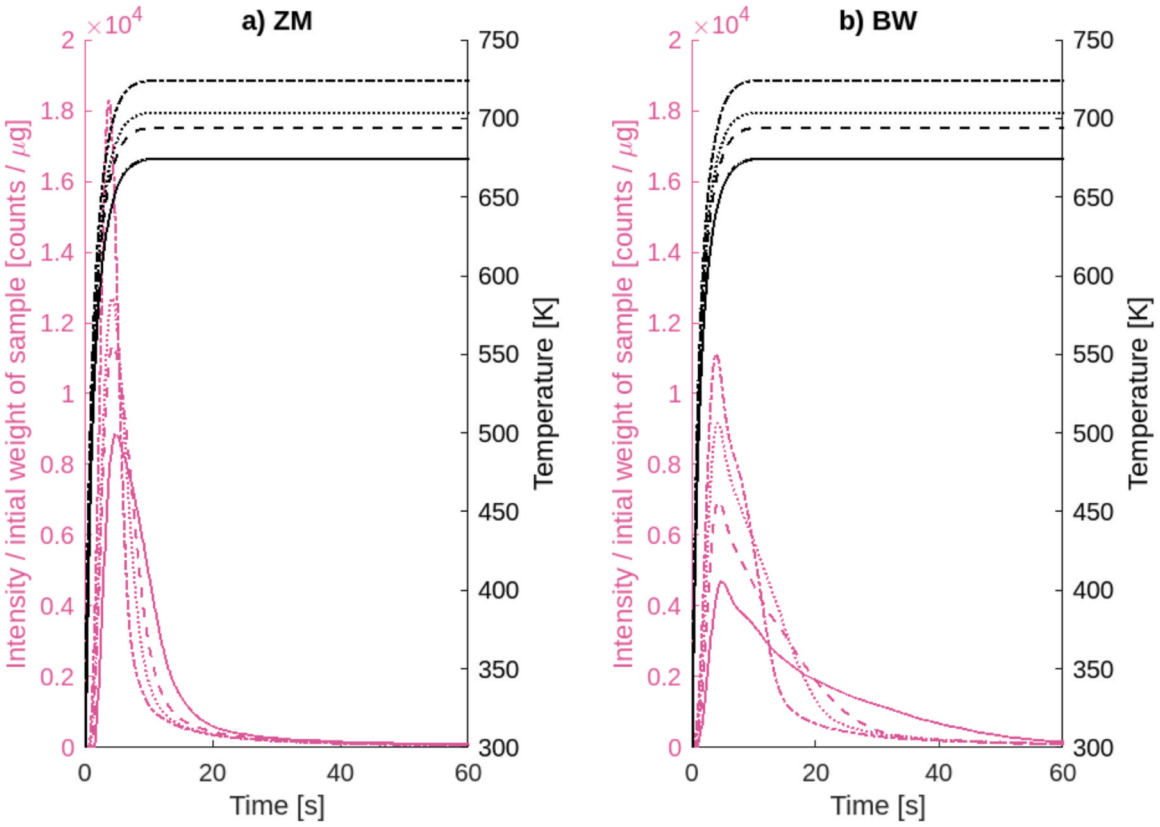

Fig. 5. Real-time devolatilization profiles and T(t) profiles at several furnace temperatures (– $T_{furnace}$ = 400 °C, – $T_{furnace}$ = 420 °C, … $T_{furnace}$ = 430 °C, and -.- $T_{furnace}$ = 450 °C) for a) *Zea Mays* leaves (ZM) and b) Beechwood (BW).

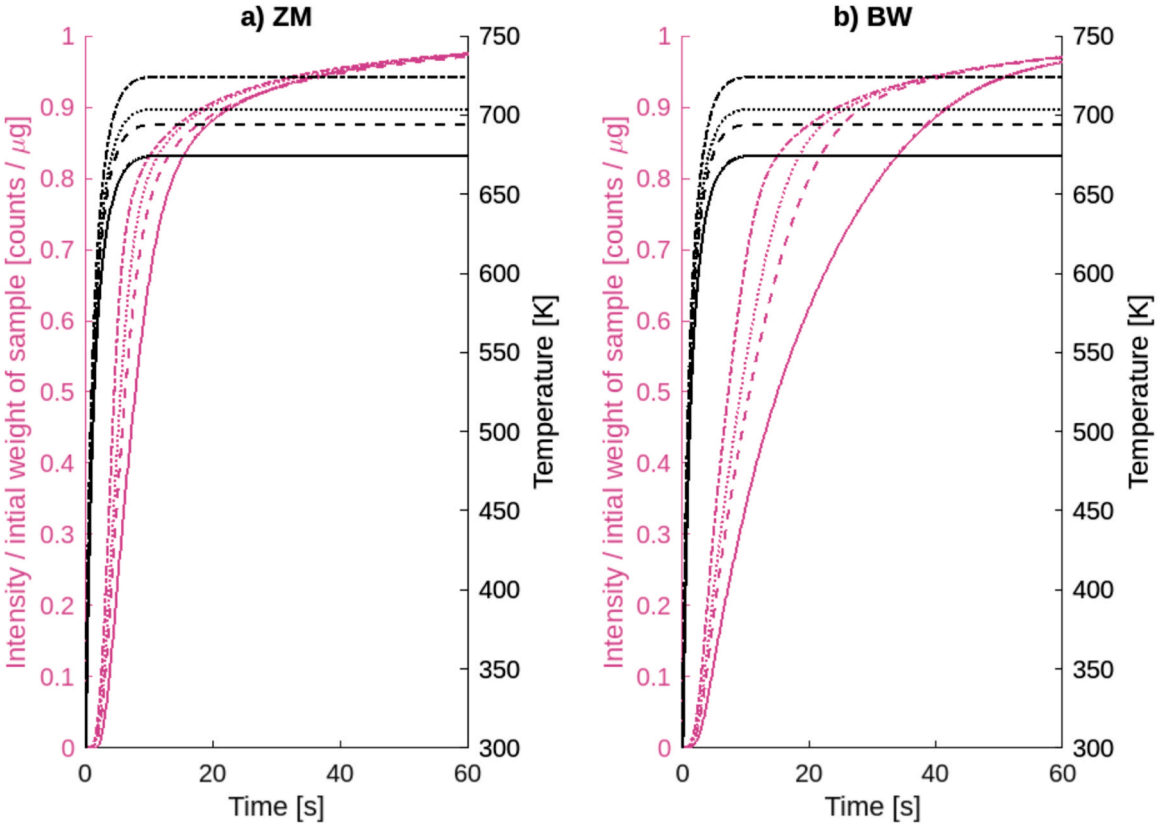

Fig. 6. Conversion curves (on the left) for a) *Zea Mays* leaves (ZM) and b) Beechwood (BW) devolatilization and T(t) profiles (on the right) obtained at several furnace temperatures (– $T_{furnace}$ = 400 °C, (- $T_{furnace}$ = 420 °C, … $T_{furnace}$ = 430 °C, and -.- $T_{furnace}$ = 450 °C).

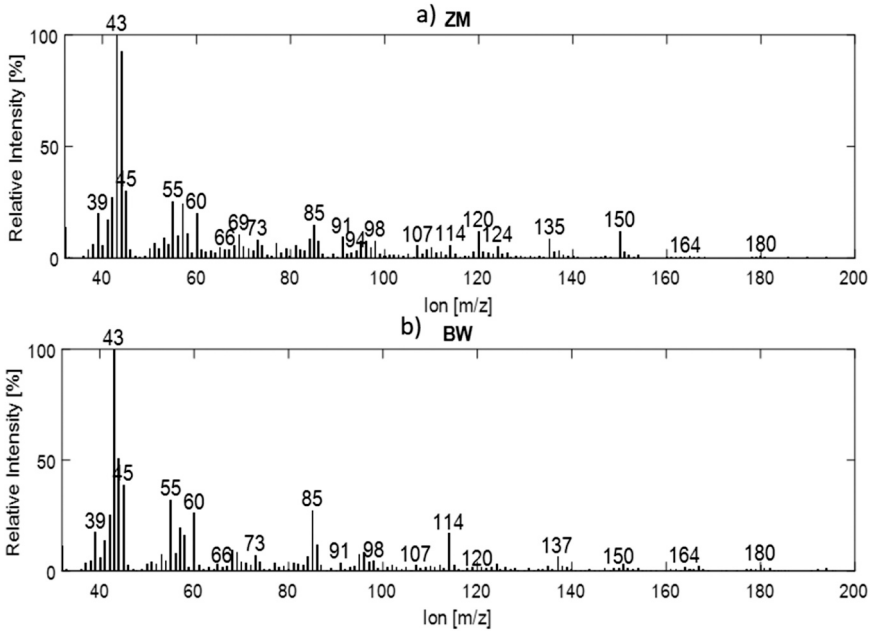

Fig. 7. Average mass spectrum ZM (a) and BW (b) at $T_{furnace}$ = 430 °C.

product distribution [58–60]. Their presence inhibits holocellulose depolymerization via transglycosylation, producing mainly levoglucosan, anhydrosugars, and oligomers. At the same time, it promotes ring fragmentation reactions, which leads to low molecular weight compounds (e.g., acetol, hydroxyacetaldehyde, formaldehyde, and furan-ring derivatives) [61]. In our case, peaks at *m/z* 60 and 73 confirm the presence of levoglucosan but are less significant than the signal at *m/z* 43, which could prove the catalytic effect of alkali inorganics during biomass pyrolysis. The fragment at *m/z* 60 can also be related to the presence of aliphatic carbon acids (e.g., acetic acid or glycolaldehyde) from hemicelluloses pyrolysis [62]. Carbon dioxide (*m/z* 44) is one of the most predominant fragments, and its formation is found to be more prominent for ZM pyrolysis than that of BW (Fig. 7). However, using the MS spectrum, it is not easy to distinguish between CO_2 released during the pyrolysis process and that produced from the electron ionization of other pyrolysis compounds. Chromatograms obtained using Py-GC-MS/FID also showed an intense peak at the elution time of CO_2, confirming that the high ash content within ZM could have promoted CO_2 formation via decarboxylation and led to an intense peak [48]. Some specifically identified peaks are related to holocellulose pyrolysis products, such as aliphatic carbon acids (e.g., formic acid with *m/z* 45), some aldehydes (*m/z* 55), ketones (e.g., acetone with *m/z* 57), cyclopentanone derivatives (*m/z* 69), furanones from cellulose (*m/z* 85), furylcarbonyl-derivatives (*m/z* 95 and 96), and anhydrosugars (*m/z* 114) [13,63–65], which relative intensity changes according to their botanical origin (Table B.1 in supplementary material, section B). Lignin reactivity is also affected by the type of chemical bonds and functional groups [33]. Peaks at *m/z* 124, 135, 137, 150, and 164 are typical markers of the guaiacyl lignin monomeric unit (G) [66–69], and those at *m/z* 154 and 167, 180, and 181 are derived from the syringyl lignin monomeric unit (S) [65,69,70]. Finally, the p-hydroxyphenyl unit (H) produces phenol derivatives products associated with *m/z* ratios of 66, 91, 94, 107, and 120 [67,70].

The difference in lignin structure between *Zea Mays* leaves (ZM) and beechwood (BW) can also be observed by using MS spectra (Fig. 7). Higher signal intensities of syringyl derivatives, a typical feature of hardwoods, are obtained for BW, while phenol derivatives (e.g., 4-vinylphenol with *m/z* 120) are strong markers for ZM. No significant signals were detected above *m/z* 200 (not shown here), which can be related to the technical limitation of the experimental system of effectively capturing and analyzing high molecular weight compounds with a boiling point above 300 °C.

Based on the detection and identification of those *m/z* ratios, intensity profiles of each extracted ion were possible and provided in Supplementary material, section J. Those extracted ion profiles were summed up to evaluate the contribution of holocellulose and lignins fractions during the overall biomass pyrolysis (Fig. 8). For beechwood (BW), the decomposition of holocellulose begins first, followed by lignins. Holocellulose for BW presents a principal peak with a late peak shoulder. The first peak cannot be only attributed to the presence of hemicelluloses. However, its decomposition is known to start before cellulose [71] because this latter is the main component of BW (47.9 wt %), and it is supposed to release more volatile matters resulting in a more intense peak. The selection of the heating rate range affects the shape of derivative thermogravimetric peaks [72], and heat/mass transfer limitations within particles are often invoked to explain peak shifts. Under fast heating, ion profiles corresponding to the simultaneous degradation of holocellulose and lignins highly overlap (Fig. 8).

In the case of ZM pyrolysis, one prominent peak is detected, corresponding to the simultaneous decomposition of holocellulose and lignins. The catalytic effect of potassium could also enhance the overlap of those three main components [73]. The combined areas of both selected ion profiles of holocellulose and lignins (Fig. 8, dashed line) represent approximately 40% of the total area underneath the devolatilization profile of whole biomass, which is relatively limited. Indeed, to discriminate the thermal behavior between main components, common ion fragments (e.g., *m/z* 44, Fig. 7) could not be extracted.

3.2. *Isoconversional E_α trends for product formation*

The methodologies mentioned above have allowed the reliable extraction of real-time devolatilization profiles of overall biomass and its main components. Studying global kinetics and, more specifically, the variation of the effective activation energy, E_α, versus the extent of conversion, α, is now possible. This latter is a powerful tool for identifying major pathways and establishing lumped reactional networks. However, reliable computational data must be obtained first. Fig. 9 shows the impact of considering the 'real' temperature-time history or/and retention time distribution on the determination of effective isoconversional activation energy, in particular for BW devolatilization

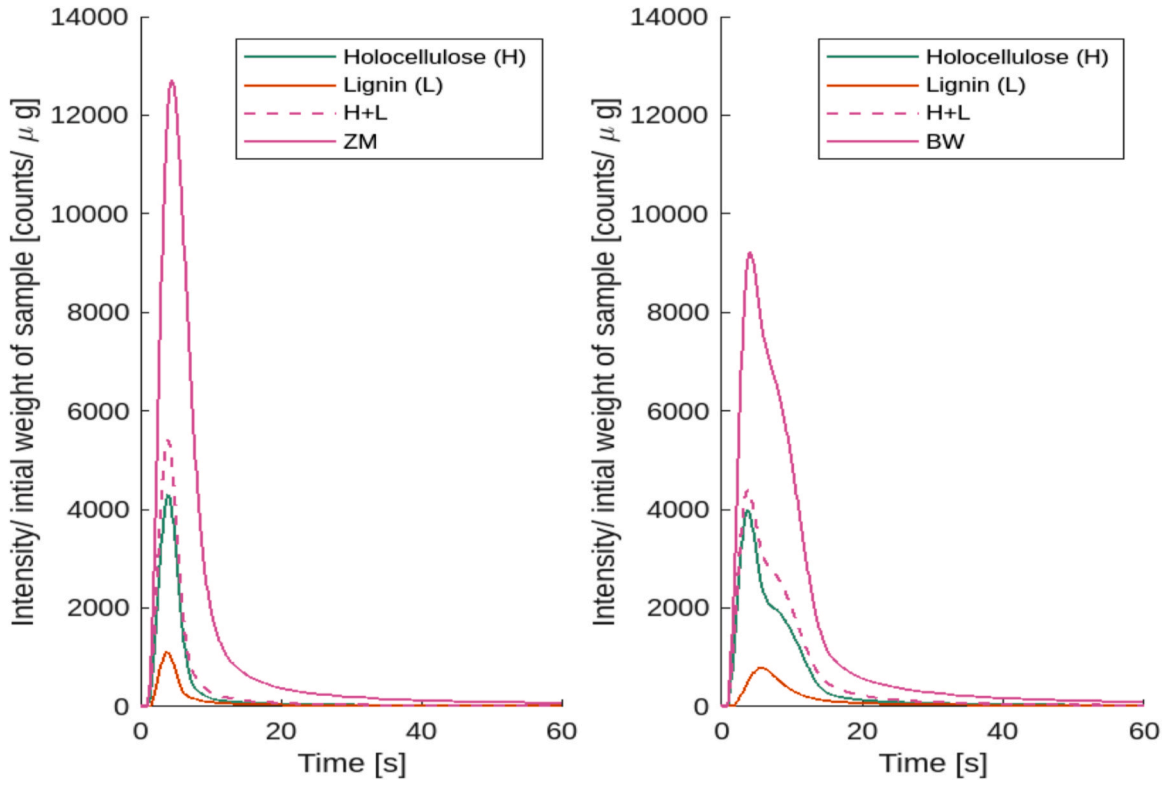

Fig. 8. Real-time devolatilization profiles for whole biomass (pink curve), holocellulose-H (green curve), and lignins-L(orange curve), for ZM (a) and BW (b) at $T_{furnace} = 430\ ^{\circ}C$. Curves of holocellulose and lignins are summed to obtain the pink dashed curve.

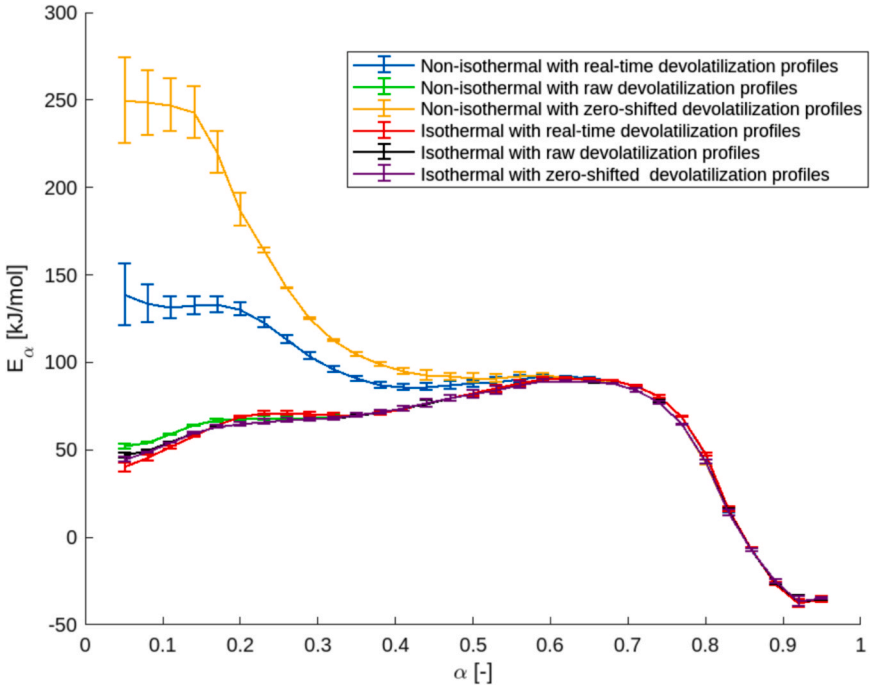

Fig. 9. Determined activation energies, $E_{\alpha,}$ for the devolatilization of beechwood. The blue, green, and yellow curves were obtained using the deconvoluted real-time, raw, and zero-shifted biomass devolatilization profiles, respectively, incorporating the temperature profile of the biomass sample. The red, black, and purple curves were obtained using the deconvoluted real-time, raw, and zero-shifted biomass devolatilization profiles, respectively, assuming isothermal experiments. The error bars are calculated based on two data sets under the same experimental conditions, which reflects the reproducibility testing.

(Fig. 9). By referring to curves obtained using real-time profiles (Fig. 9, blue and purple curves), we can deduce that the hypothesis of the isothermal experiment strongly impacts the inferred activation energies; at the beginning of conversion, for example, the activation energy decreases from approximately 145 to 49 kJ/mol for non-isothermal and isothermal conditions, respectively. As mentioned before, more than 30% of conversion is reached during heating. While in isothermal conditions, the temperature is assumed to be constant during this stage, leading to a false estimate of activation energy during the heating period. Not correcting the devolatilization profiles (black and green curves) has a comparable impact on the activation energy predictions to the isothermal hypothesis. The classical correction of the

devolatilization profile (yellow curve) consisting of a simple zero-shifting is not satisfactory as well as it leads to an overestimation of the activation energy values during the heating period ($\alpha < 0.4$). Those results confirm that inadequate data collection can lead to drastic errors.

Graphical trends of the effective activation energies obtained for *Zea Mays* leaves (ZM), beechwood (BW), and their components (holocellulose and lignins) are presented in Fig. 10. It displays the substantial variability of effective activation energy values when it comes to assessing the thermal reactivity of both biomass samples and their main components, depicting the complex nature of their fast pyrolysis transformation.

It is important to note that the linear fit of isoconversional points, represented by the mean of the linear regression coefficient (R^2), was not good for both low and high conversion. This indicates significant errors when estimating activation energies, as shown in the gray zones in Fig. 10. Similar errors associated with linear regression have been reported in other papers [74–76]. There can be several reasons for this 'imperfect' linear regression in isoconversional methods:

- Insufficient or noisy experimental data can lead to inaccurate linear regression results, affecting the overall accuracy of the method.
- The occurrence of multi-step reactions during biomass pyrolysis can also contribute to imperfect linear regression. It is important to note that isoconversional methods describe the pyrolysis process using several single-step reaction kinetic equations, each associated with a certain extent of conversion. However, in some cases, the assumption of single-step reactions may not hold true, leading to deviations and inaccuracies in the method accuracy.
- Changes in the reaction steps can result in drastic variations in the slope of the isoconversional line. It can be pointed out that if all isoconversional lines have the same slope, only one mechanism with one apparent activation energy is inferred. Any variation of the slope of the isoconversional lines indicates that at least two different mechanisms with distinct apparent activation energies are involved.

In our case, the end of the process is characterized by a decrease in ln (dα/dt) with increasing temperature. Because of this behavior, the

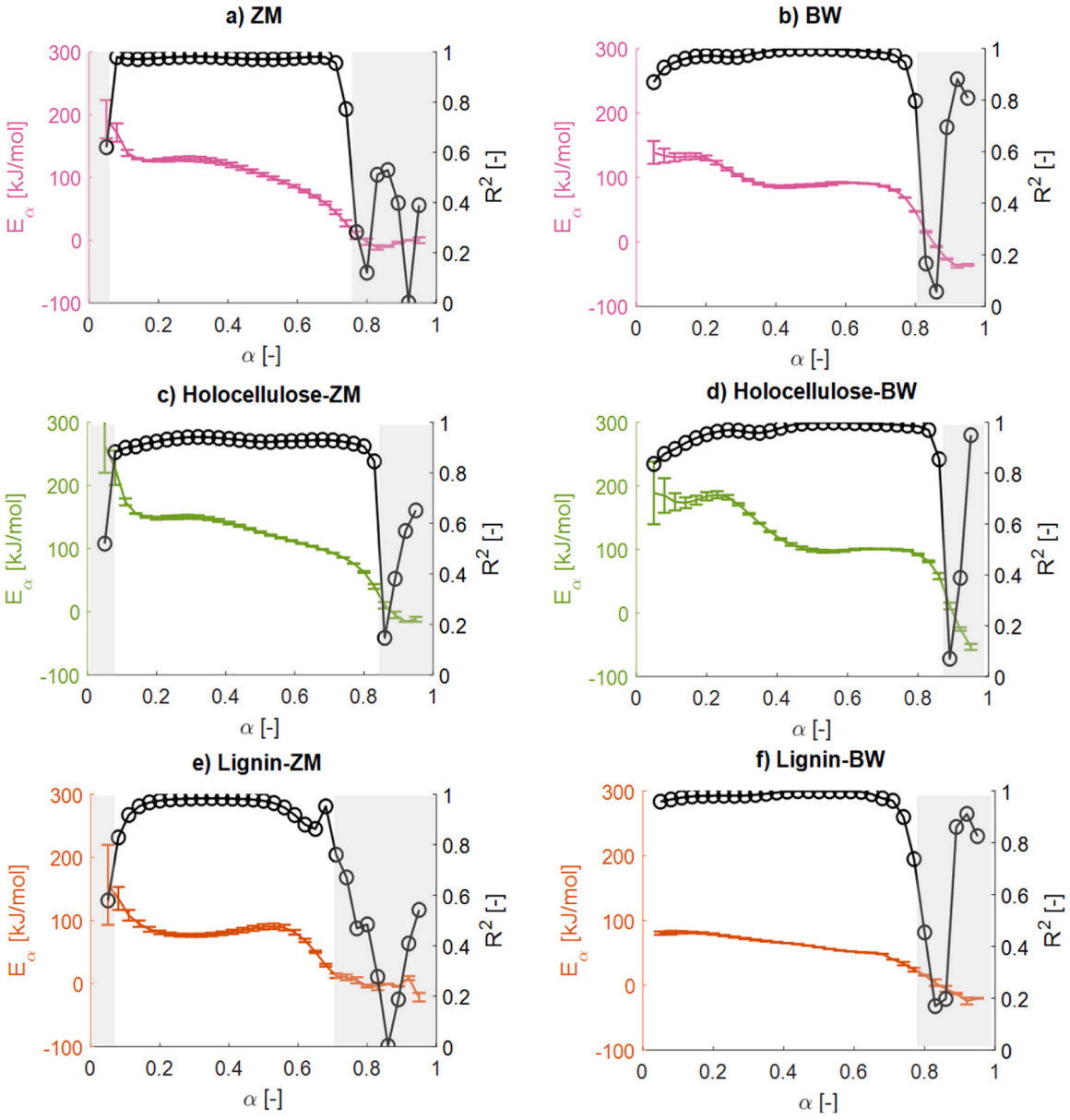

Fig. 10. E_α vs. α for a) ZM, b) BW, c) holocellulose of ZM, d) holocellulose of BW, e) lignins of ZM, and f) lignins of BW. R^2 is the linearization coefficient. The error bars are derived from two data sets obtained under identical experimental conditions, demonstrating the reproducibility testing.

calculated slope of the straight line of this region would be positive, resulting in a negative activation energy value. This drastic change in the slope of the isoconversional lines (Fig. K.1 in Supplementary material, section K) is manifested by a sudden decrease in the regression coefficient value (Fig. 10). Then, linear regression coefficients start to have higher values towards the end (0.9 for BW, and 0.6 for ZM).

Considering E_α vs. α curves outside the gray zones, different decomposition elementary steps with activation energies that vary according to the extent of conversion for two biomass samples are observed. When interpreting an isoconversional E_α curve, it is important to understand that each plateau can be assigned an elementary reaction, an initial guess for selecting kinetic models. Here, under fast heating, a gradual decrease of E_α values is observed for both biomasses and related components (Fig. 10), a potential indication of the process limiting step changing. During BW pyrolysis, two plateaus are observed at $E_{\alpha,1} \approx 140$ kJ/mol and $E_{\alpha,2} \approx 90$ kJ/mol for the whole material and at $E_{\alpha,1} \approx 180$ kJ/mol, and $E_{\alpha,2} \approx 100$ kJ/mol those for its holocellulose. Those features can be related to two different reactional steps that are in competition between $0.2 < \alpha < 0.4$ for BW and $0.25 < \alpha < 0.45$ for its holocellulose fraction. For the grassy material (ZM), all E_α trends decrease and display, in general, higher energy barriers at the beginning compared to those of wood. For ZM, only one plateau between $0.2 < \alpha < 0.4$ is observed. The higher ash content in ZM enhances the char formation process, shown by higher char yields than BW (from 9.6 $\pm$ 0.5 wt% at T = 450 °C to 16.6 $\pm$ 0.3 wt% at T = 400 °C for ZM and from 6.8 $\pm$ 0.3 wt% at T = 450 °C to 15.4 $\pm$ 0.2 at T = 400 °C for BW).

Unsurprisingly, E_α variation for ZM lignins differed from that of BW lignins as the chemical nature of grass-derived lignins is much more complex than those of wood-derived lignins [33]. The thermal reactivity of grass-derived lignins is generally lesser than that of hardwood-derived lignins, which is in good correspondence with our work ($E_{\alpha,grass} > E_{\alpha,wood}$). It is also important to stress that for this study, the values of effective activation energies are representative of the production of the low molecular weight fractions. This could be particularly problematic for lignins as the formation of heavier compounds, such as lignin dimers and oligomers, having higher boiling points cannot overcome the temperature limitation fixed at 300 °C by the GC injection port.

Comparing our results to those from the literature is challenging due to the considerable disparity between experimental setups, operating conditions, and calculation methodologies [77].

Due to challenges in understanding and underlying the chemistry of biomass pyrolysis [9], typical and wide ranges of activation energy are found: 97–208 kJ/mol for cellulose [26,44,78–80], 70–200 kJ/mol for hemicelluloses [80–83], and 33–260 kJ/mol for lignins [81,82,84–86]. An even wider range is expected when considering the whole biomass: 70–211 kJ/mol and 60–180 kJ/mol, respectively, for grassy and woody feedstocks [77,79,87]. The works that claimed the kinetic rate-controlled regime of fast pyrolysis are of particular interest. For example, Zhu et al. [78] found an activation energy of 97.1 kJ/mol for cellulose conversion between 385 and 467 °C using a PHASR reactor, and the work of Di Blasi and Branca [87] reported an activation energy of 141 kJ/mol for beechwood fast pyrolysis between 300 and 435 °C. E_α values found in this work were comparable to those previously reported.

3.3. Comparative pyrolysis kinetics based on VAEM and DAEM approaches

The short simplification of single-step first-order reaction could not capture the complex nature of biomass devolatilization reactions as described in Supplementary material, section L. In this section, devolatilization rates of both *Zea Mays* leaves (ZM) and beechwood (BW) determined based on Py-MS data at different sample temperature histories were further tested with two different reactivity kinetic models: the variable activation energy model (VAEM) and the distributed activation energy model (DAEM). Unknown parameters were determined from the model fitting (Tables M.1 and M.2 in Supplementary material, section M).

The models reproduce the experimental data with high precision ($reldev_8 < 3\%$) in this descending order: VAEM, 2 G-DAEM, and 1 G-DAEM for both biomass samples, as shown in Figs. M.1 to M.6 in Supplementary material, section M. This confirms that the two types of models, whether the VAEM describing the biomass devolatilization as "infinitely sequential reactions" or the DAEM describing the complex reaction system as "infinitely parallel reactions," are suitable for the accurate prediction of the biomass pyrolysis behavior. The VAEM still retains the advantage of not assuming any form of the reaction model and therefore avoids errors related to the choice of reaction model, while DAEM double Gaussian may provide further insights in terms of phenomenology. VAEM contains more parameters (twelve for VAEM vs. seven for 2 G-DAEM). However, in kinetic modelling, it is essential to select a kinetic model which reasonably represents the pyrolysis process without too many parameters to prevent overfitting. To detect overfitted data, the prerequisite is that it must be used on test data. In this study, obtained model parameters were tested to another experimental data set acquired at $T_{furnace} = 440$ °C (Fig. N.1 in Supplementary material, section N). The relative deviation between the experimental data and those calculated for this test dataset ($reldev_{test} = 0.95$ for ZM and 1.88 for BW) was comparable to those obtained based on the training data set ($reldev_8 = 1.43$ for ZM and 1.26 for BW), confirming the absence of overfitting in the model.

From the comparison of numerical values between kinetic parameters (Table M.1 in Supplementary material, section M), the effective activation energies determined for whole biomass devolatilization using 1 G-DAEM are around 117 kJ/mol for ZM and 119 kJ/mol for BW. The found values are lower than those reported in the literature for a first-step reaction, 141 kJ/mol and 150 kJ/mol, reported respectively by Di Blasi and Branca [87] for beechwood and Wagenaar et al. [88] for pine. The maximum devolatilization rate increased from only 0.1–0.22 s^{-1} for ZM and from 0.05 to 0.11 s^{-1} for BW when varying the furnace temperature (and therefore varying the heating rate). This relatively small rate increase suggests that the effective activation energy is smaller than that of previous studies. The obtained activation energies are comparable to that measured by Zhu et al. [78] for α-cyclodextrin (97.1 kJ/mol) using the PHASR reactor known for its ability to establish an intrinsic kinetic regime. Using this same reactor, Maduskar et al. [17] measured the formation kinetics of six key molecules (levoglucosan, furfural, hydroxymethylfurfural, 2-methoxyphenol, 2-methoxy4-methylphenol, and 2-methoxy-4-vinylphenol) of loblolly pine pyrolysis. The wide range of values (70–186 kJ/mol) is comparable to the apparent activation values found in this study, 117 and 119 kJ/mol for BW and ZM, respectively. Notably, this highlights the importance of instrument lag corrections (temperature profile and devolatilization profiles). Indeed, ignoring these elements would lead to erroneous kinetics.

Considering the 2 G-DAEM, the second pyrolysis step is confined to a lower value of activation energy (E_2 = 74.04 kJ/mol for ZM and 89.98 kJ/mol for BW). This step is essentially due to the fast devolatilization of lignins. Although lignin consists of cross-linked aromatic macromolecules, and its decomposition requires more energy to be accomplished, in our case, the determined kinetics are only related to the formation of light molecules as our system only screens low boiling point molecules. The parameters c_1 and c_2 for the 2 G-DAEM assume particular importance since it identifies the dominant pyrolysis step. The c_2 values are relatively low (0.03 for ZM and 0.09 for BW), indicating that the primary step is the dominant mechanism. Furthermore, the contribution of the second step is lower than the lignin initial mass fraction in biomass, confirming that this step is only related to a part of lignin devolatilization. The first pyrolysis step with higher contribution can be attributed mainly to holocellulose degradation.

3.4. E_{VAEM} curves

The VAEM fitting to the experimental data for biomass samples (Figs. M.5 and M.6 in Supplementary material, section M) and their components (Figs. O.1 and O.2 in Supplementary material, section O) make it possible to determine the optimal parameters of the E_α functions (Tables M.2 and O.1 in Supplementary material). The difference between E_{VAEM} curves and isoconversional activation energy E_α is more evident at the earlier conversions and in the tail zone, while the mid zone is almost the same for both.

As isoconversional activation energy values were marred by errors related to the bad regression at the beginning and the end of the pyrolysis process (Fig. 11) and VAEM curves are determined from experimental data fitting, make these later more accurate. Thus, adequate mechanistic interpretations are permitted from them.

The activation energy values at zero conversion prevail in the initial pyrolysis stage. As the whole biomass and holocellulose devolatilizations start at almost the same activation energy values (Fig. 11) for both types of biomass, the initial stage can only be linked to the degradation of one of the holocellulose components, probably to hemicelluloses, which is more reactive than cellulose. The two consecutive plateaus at 130 and 90 kJ/mol for BW holocellulose could be associated with cellulose degradation, which generally includes two steps starting with its depolymerization into an active intermediate, the "active cellulose," which laterally undergoes competitive reactions to produce char and gas or primary volatiles [89].

The participation of each major component is different for each type of biomass. Holocellulose degradation was prominent at $\alpha < 0.1$ and $\alpha < 0.25$ for BW and ZM devolatilization, respectively, as the activation energy values for these stages are comparable to those obtained for whole biomass.

For conversion stages between $0.1 < \alpha < 0.5$ for BW and $0.1 < \alpha < 0.5$ for ZM, both holocellulose and lignins participate in devolatilization. For further conversion, holocellulose predominates in BW devolatilization, while lignin contribution becomes more significant in ZM devolatilization. The high ash content of ZM may affect more severely the second degradation stage of cellulose (starting from $\alpha = 0.4$), thus catalyzing the overall reaction, which was faster, $d\alpha/dt = 0.21\ s^{-1}$ at 450 °C (Fig. M.5. in Supplementary material, section M) against $d\alpha/dt = 0.1\ s^{-1}$ at 450 °C (Fig. M.6. in Supplementary material, section M) for BW.

Negative activation energy values, until − 150 kJ/mol, were obtained at the end of the process ($\alpha > 0.88$). If negative activation energies have already been reported in the literature [90], it remains a little-known fact. Certain gas-phase reactions have been shown to have activation energies near zero or even negative [91]. In our study, those negative activation energies (Fig. 11) are obtained at the end of the process (therefore, in the presence of residual solids) and under isothermal conditions (see Supplementary material, section K). The decrease in E_α could be explained by a shift of the process-determining step [92] and most probably with exothermic char-forming reactions catalyzed by minerals with biochar and characterized by intrinsic negative activation energy [93,94]. However, further investigation is required to support this suggestion.

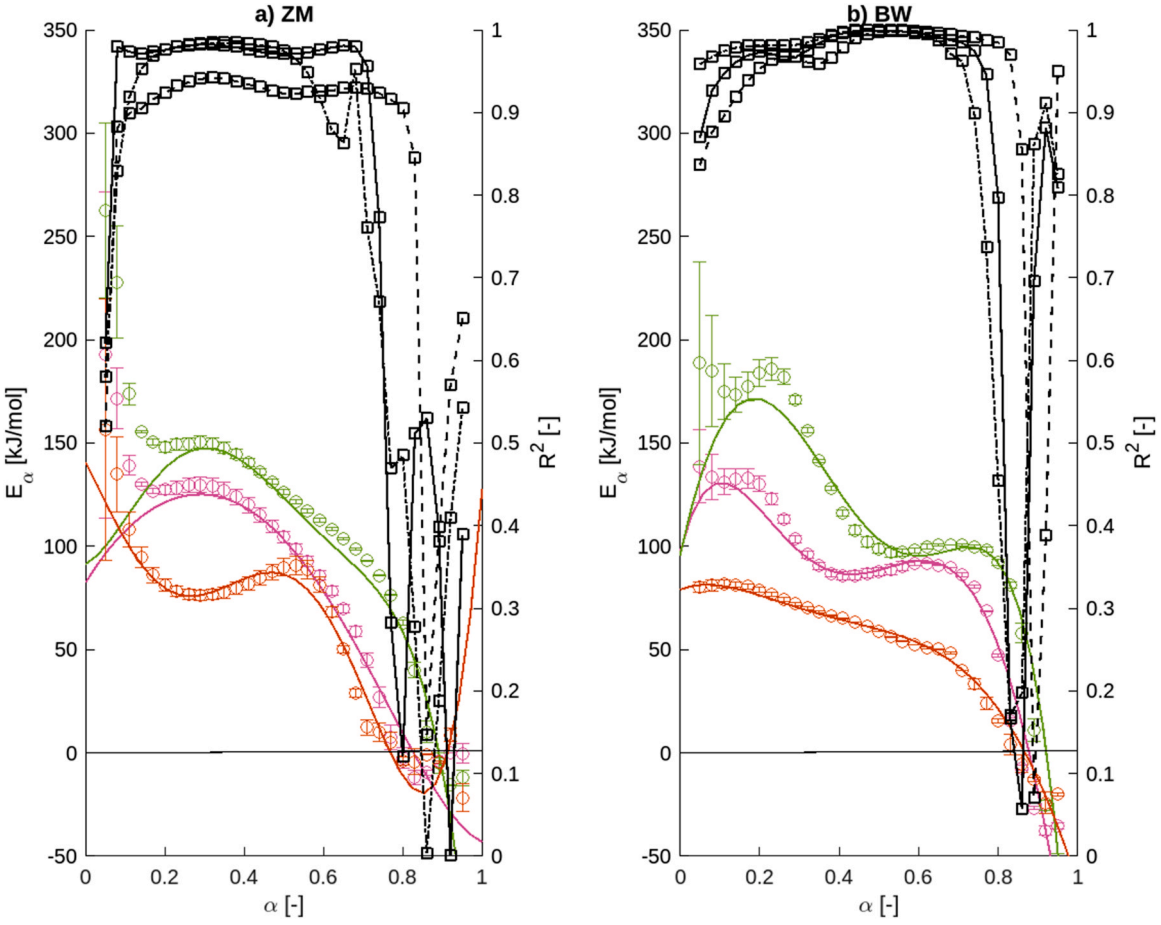

Fig. 11. Comparison of isoconversional E_α (symbols) to those approximated by fifth-order polynomials in the empirical model (continuous lines) for ZM (a), BW (b), and their pseudo-compounds. Pink is used for the whole biomass, green for holocelluloses, and orange for lignins. The right axis represents the coefficient associated with linear regressions of the Freidman method (Lines connecting symbols are distinct for biomass (-), holocelluloses (–), and lignins (-.-)).The error bars represent the variation between two data sets collected under identical experimental conditions, indicating the reproducibility of the results.

4. Conclusions

Online analysis techniques like the micropyrolyzer coupled to the mass spectrometer (Py-MS) used in this study are essential to follow the dynamics of volatile formation during biomass decomposition, making the commercial micropyrolyzer used not only for product identification and quantification but also to evaluate fast pyrolysis kinetics. In addition to the whole biomass devolatilization, those related to its main fractions (holocellulose and lignins) were determined directly by extracting the appropriate *m/z* ratios.

However, inadequate data collection can introduce drastic errors in kinetic parameter determination, highlighting oversights by previous researchers. In particular, calculations should be performed before experimentation to determine experimental conditions ensuring a kinetically controlled regime and the true sample temperature profile and real-time devolatilization profile should be determined for proper kinetic derivation.

The isoconversional method, combined with the true temperature history of the biomass sample, was applied to the deconvoluted devolatilization profiles. Effective activation energies highly varied for both beechwood (<-50 to 140 kJ/mol) and *Zea mays* leaves (−40 to 240 kJ/mol), confirming the multi-step nature of the fast pyrolysis process.

Although a first-order reaction model is essential for global reactivity comparison between different types of fuels, it can hardly capture the complexity of biomass devolatilization. Both VAEM and DAEM ensure a moderate representation of biomass heterogeneity and pyrolysis complexity. The VAEM retains the advantage of studying biomass devolatilization without assuming mathematical form for the reactional model, f(α). However, DAEM double Gaussian may provide further insights regarding phenomenology and biopolymers contribution.

Examining optimized E_{VAEM} trends confirms the presence of exothermic char-forming reactions at the end of the pyrolysis process, which is characterized by an E_α near zero, even negative. The optimized E_{VEAM} curves were not similar for woody and grassy biomass, confirming the different behavior of their devolatilization. Therefore, a generalization of parameters was not possible for biomass devolatilization modelling, whatever the type of biomass, indicating the need for further kinetic investigation considering the botanical origin of biomasses.

Declaration of Competing Interest

The authors declare the following financial interests/personal relationships which may be considered as potential competing interests: Marion Carrier reports financial support was provided by Occitanie Region. Marion Carrier reports financial support was provided by French National Research Agency.

Data Availability

All codes can be found in the supplementary data.

Acknowledgments

The authors acknowledge the French scientific program MOPGA (reference ANR-18-MPGA-0013), managed by the National Research Agency and financially supported by the "Investissements d'Avenir" and Region Occitanie (18016004). We acknowledge the helpful pieces of advice of Dr. Jean-Louis Dirion and the reviewers for their thoughtful comments and efforts towards improving our manuscript.

Appendix A. Supporting information

Supplementary data associated with this article can be found in the online version at doi:10.1016/j.jaap.2023.106128.

References

[1] L. Zhang, C. (Charles) Xu, P. Champagne, Overview of recent advances in thermochemical conversion of biomass, Energy Convers. Manag 51 (2010) 969–982, https://doi.org/10.1016/j.enconman.2009.11.038.
[2] S. Xiu, A. Shahbazi, Bio-oil production and upgrading research: a review, Renew. Sustain Energy Rev. 16 (2012) 4406–4414, https://doi.org/10.1016/j.rser.2012.04.028.
[3] X. Hu, M. Gholizadeh, Progress of the applications of bio-oil, Renew. Sustain Energy Rev. 134 (2020), 110124, https://doi.org/10.1016/j.rser.2020.110124.
[4] D. Beneroso, T. Monti, E.T. Kostas, J. Robinson, Microwave pyrolysis of biomass for bio-oil production: Scalable processing concepts, Chem. Eng. J. 316 (2017) 481–498, https://doi.org/10.1016/j.cej.2017.01.130.
[5] T.M.H. Dabros, M.Z. Stummann, M. Høj, P.A. Jensen, J.-D. Grunwaldt, J. Gabrielsen, et al., Transportation fuels from biomass fast pyrolysis, catalytic hydrodeoxygenation, and catalytic fast hydropyrolysis, Prog. Energy Combust. Sci. 68 (2018) 268–309, https://doi.org/10.1016/j.pecs.2018.05.002.
[6] G. Perkins, T. Bhaskar, M. Konarova, Process development status of fast pyrolysis technologies for the manufacture of renewable transport fuels from biomass, Renew. Sustain Energy Rev. 90 (2018) 292–315, https://doi.org/10.1016/j.rser.2018.03.048.
[7] K.B. Ansari, J.S. Arora, J.W. Chew, P.J. Dauenhauer, S.H. Mushrif, Fast pyrolysis of cellulose, hemicellulose, and lignin: effect of operating temperature on bio-oil yield and composition and insights into the intrinsic pyrolysis chemistry, Ind. Eng. Chem. Res 58 (2019) 15838–15852, https://doi.org/10.1021/acs.iecr.9b00920.
[8] A.V. Bridgwater, Review of fast pyrolysis of biomass and product upgrading, Biomass-.-. Bioenergy 38 (2012) 68–94, https://doi.org/10.1016/j.biombioe.2011.01.048.
[9] M.S. Mettler, D.G. Vlachos, P.J. Dauenhauer, Top ten fundamental challenges of biomass pyrolysis for biofuels, Energy Environ. Sci. 5 (2012) 7797, https://doi.org/10.1039/c2ee21679e.
[10] S. Singh, C. Wu, P.T. Williams, Pyrolysis of waste materials using TGA-MS and TGA-FTIR as complementary characterisation techniques, J. Anal. Appl. Pyrolysis 94 (2012) 99–107, https://doi.org/10.1016/j.jaap.2011.11.011.
[11] H. Yang, R. Yan, T. Chin, D.T. Liang, H. Chen, C. Zheng, Thermogravimetric analysis−fourier transform infrared analysis of palm oil waste pyrolysis, Energy Fuels 18 (2004) 1814–1821, https://doi.org/10.1021/ef030193m.
[12] J. Giuntoli, S. Arvelakis, H. Spliethoff, W. de Jong, A.H.M. Verkooijen, Quantitative and kinetic thermogravimetric fourier transform infrared (TG-FTIR) study of pyrolysis of agricultural residues: influence of different pretreatments, Energy Fuels 23 (2009) 5695–5706, https://doi.org/10.1021/ef9005719.
[13] G. Lv, S. Wu, Analytical pyrolysis studies of corn stalk and its three main components by TG-MS and Py-GC/MS, J. Anal. Appl. Pyrolysis 97 (2012) 11–18, https://doi.org/10.1016/j.jaap.2012.04.010.
[14] Z. Ma, D. Chen, J. Gu, B. Bao, Q. Zhang, Determination of pyrolysis characteristics and kinetics of palm kernel shell using TGA-FTIR and model-free integral methods, Energy Convers. Manag 89 (2015) 251–259, https://doi.org/10.1016/j.enconman.2014.09.074.
[15] A.A. Jain, A. Mehra, V.V. Ranade, Processing of TGA data: Analysis of isoconversional and model fitting methods, Fuel 165 (2016) 490–498, https://doi.org/10.1016/j.fuel.2015.10.042.
[16] M. Nasfi, M. Carrier, S. Salvador, Reconsidering the potential of micropyrolyzer to investigate biomass fast pyrolysis without heat transfer limitations, J. Anal. Appl. Pyrolysis 165 (2022), 105582, https://doi.org/10.1016/j.jaap.2022.105582.
[17] S. Maduskar, G.G. Facas, C. Papageorgiou, C.L. Williams, P.J. Dauenhauer, Five rules for measuring biomass pyrolysis rates: pulse-heated analysis of solid reaction kinetics of lignocellulosic biomass, ACS Sustain Chem. Eng. 6 (2018) 1387–1399, https://doi.org/10.1021/acssuschemeng.7b03785.
[18] E. Hoekstra, W.P.M. van Swaaij, S.R.A. Kersten, K.J.A. Hogendoorn, Fast pyrolysis in a novel wire-mesh reactor: Design and initial results, Chem. Eng. J. 191 (2012) 45–58, https://doi.org/10.1016/j.cej.2012.01.117.
[19] P. Liu, H. Zhuang, Y. Qian, J. Yang, Y. Pan, Z. Zhou, et al., Recent advances in mass spectrometric studies on the reaction process of biomass pyrolysis, Fuel Process Technol. 237 (2022), 107473, https://doi.org/10.1016/j.fuproc.2022.107473.
[20] F. Nardella, M. Mattonai, E. Ribechini, Evolved gas analysis-mass spectrometry and isoconversional methods for the estimation of component-specific kinetic data in wood pyrolysis, J. Anal. Appl. Pyrolysis 145 (2020), 104725, https://doi.org/10.1016/j.jaap.2019.104725.
[21] Y.-M. Kim, T.U. Han, B. Hwang, Y. Lee, A. Watanabe, N. Teramae, et al., New approach for the kinetic analysis of cellulose using EGA-MS, Polym. Test. 60 (2017) 12–17, https://doi.org/10.1016/j.polymertesting.2017.02.004.
[22] A.K. Burnham, L.N. Dinh, A comparison of isoconversional and model-fitting approaches to kinetic parameter estimation and application predictions, J. Therm. Anal. Calor. 89 (2007) 479–490, https://doi.org/10.1007/s10973-006-8486-1.
[23] Phusunti N., Hornung A. Formal Kinetic Parameters – Problems and Solutions in Deriving Proper Values 2014:257–284. https://doi.org/10.1002/9781118693643.ch14.
[24] J. Cai, W. Wu, R. Liu, An overview of distributed activation energy model and its application in the pyrolysis of lignocellulosic biomass, Renew. Sustain Energy Rev. 36 (2014) 236–246, https://doi.org/10.1016/j.rser.2014.04.052.
[25] A.K. Burnham, Introduction to chemical kinetics, in: A.K. Burnham (Ed.), Glob. Chem. Kinet. Foss. Fuels Model Matur. Pyrolysis, Springer International Publishing, Cham, 2017, pp. 25–74, https://doi.org/10.1007/978-3-319-49634-4_2.
[26] M. Carrier, L. Auret, A. Bridgwater, J.H. Knoetze, Using apparent activation energy as a reactivity criterion for biomass pyrolysis, Energy Fuels 30 (2016) 7834–7841, https://doi.org/10.1021/acs.energyfuels.6b00794.

[27] J. Cai, D. Xu, Z. Dong, X. Yu, Y. Yang, S.W. Banks, et al., Processing thermogravimetric analysis data for isoconversional kinetic analysis of lignocellulosic biomass pyrolysis: Case study of corn stalk, Renew. Sustain Energy Rev. 82 (2018) 2705–2715, https://doi.org/10.1016/j.rser.2017.09.113.

[28] L. Luo, X. Guo, Z. Zhang, M. Chai, Md.M. Rahman, X. Zhang, et al., Insight into pyrolysis kinetics of lignocellulosic biomass: isoconversional kinetic analysis by the modified friedman method, Energy Fuels 34 (2020) 4874–4881, https://doi.org/10.1021/acs.energyfuels.0c00275.

[29] S. Vyazovkin, A.K. Burnham, L. Favergeon, N. Koga, E. Moukhina, L.A. Pérez-Maqueda, et al., ICTAC Kinetics Committee recommendations for analysis of multi-step kinetics, Thermochim. Acta 689 (2020), 178597, https://doi.org/10.1016/j.tca.2020.178597.

[30] N. Sbirrazzuoli, Interpretation and physical meaning of kinetic parameters obtained from isoconversional kinetic analysis of polymers, Polymers 12 (2020) 1280, https://doi.org/10.3390/polym12061280.

[31] C. Diblasi, Modeling chemical and physical processes of wood and biomass pyrolysis, Prog. Energy Combust. Sci. 34 (2008) 47–90, https://doi.org/10.1016/j.pecs.2006.12.001.

[32] M. Carrier, A. Loppinet-Serani, D. Denux, J.-M. Lasnier, F. Ham-Pichavant, F. Cansell, et al., Thermogravimetric analysis as a new method to determine the lignocellulosic composition of biomass, Biomass-.-. Bioenergy 35 (2011) 298–307, https://doi.org/10.1016/j.biombioe.2010.08.067.

[33] S. Wang, G. Dai, H. Yang, Z. Luo, Lignocellulosic biomass pyrolysis mechanism: a state-of-the-art review, Prog. Energy Combust. Sci. 62 (2017) 33–86, https://doi.org/10.1016/j.pecs.2017.05.004.

[34] V. Dhyani, T. Bhaskar, A comprehensive review on the pyrolysis of lignocellulosic biomass, Renew. Energy 129 (2018) 695–716, https://doi.org/10.1016/j.renene.2017.04.035.

[35] Y. Picó, D. Barceló, Pyrolysis gas chromatography-mass spectrometry in environmental analysis: Focus on organic matter and microplastics, TrAC Trends Anal. Chem. 130 (2020), 115964, https://doi.org/10.1016/j.trac.2020.115964.

[36] K.L. Sobeih, M. Baron, J. Gonzalez-Rodriguez, Recent trends and developments in pyrolysis–gas chromatography, J. Chromatogr. A 1186 (2008) 51–66, https://doi.org/10.1016/j.chroma.2007.10.017.

[37] A.K. Burnham, R.L. Braun, H.R. Gregg, A.M. Samoun, Comparison of methods for measuring kerogen pyrolysis rates and fitting kinetic parameters, Energy Fuels 1 (1987) 452–458, https://doi.org/10.1021/ef00006a001.

[38] A.E. Rodrigues, Residence time distribution (RTD) revisited, Chem. Eng. Sci. 230 (2021), 116188, https://doi.org/10.1016/j.ces.2020.116188.

[39] A.K. Burnham, Pyrolysis in Open Systems, in: A.K. Burnham (Ed.), Glob. Chem. Kinet. Foss. Fuels Model Matur. Pyrolysis, Springer International Publishing, Cham, 2017, pp. 107–169, https://doi.org/10.1007/978-3-319-49634-4_4.

[40] R.L. Braun, A.K. Burnham, Analysis of chemical reaction kinetics using a distribution of activation energies and simpler models, ACS Publ. (2002), https://doi.org/10.1021/ef00002a003.

[41] Harvey A.F., Cerna M. The Fundamentals of FFT-Based Signal Analysis and Measurement in LabVIEW and LabWindows, 1993.

[42] M. Serres, D. Schweich, V. Vidal, R. Philippe, Liquid residence time distribution of multiphase horizontal flow in packed bed milli-channel: spherical beads versus open cell solid foams, Chem. Eng. Sci. 190 (2018) 149–163, https://doi.org/10.1016/j.ces.2018.05.004.

[43] T. Liliedahl, K. Sjöström, L.-P. Wiktorsson, Analysis method of pyrolysis kinetics using modern signal processing techniques, AIChE J. 37 (1991) 1415–1419, https://doi.org/10.1002/aic.690370914.

[44] Y.-M. Kim, T.U. Han, B. Hwang, Y. Lee, A. Watanabe, N. Teramae, et al., New approach for the kinetic analysis of cellulose using EGA-MS, Polym. Test. 60 (2017) 12–17, https://doi.org/10.1016/j.polymertesting.2017.02.004.

[45] G. Várhegyi, Empirical models with constant and variable activation energy for biomass pyrolysis, Energy Fuels 33 (2019) 2348–2358, https://doi.org/10.1021/acs.energyfuels.9b00040.

[46] G. Várhegyi, P. Szabó, M.J. Antal, Kinetics of Charcoal Devolatilization, Energy Fuels 16 (2002) 724–731, https://doi.org/10.1021/ef010227v.

[47] R. Dungani, H.P.S.A. Khalil, I. Sumardi, Y. Suhaya, E. Sulistyawati, Md.N. Islam, et al., Non-wood Renewable Materials: Properties Improvement and Its Application, in: K.R. Hakeem, M. Jawaid, U. Rashid (Eds.), Biomass Bioenergy Appl, Springer International Publishing, Cham, 2014, pp. 1–29, https://doi.org/10.1007/978-3-319-07578-5_1.

[48] D.K. Ojha, D. Viju, R. Vinu, Fast pyrolysis kinetics of lignocellulosic biomass of varying compositions, Energy Convers. Manag X 10 (2021), 100071, https://doi.org/10.1016/j.ecmx.2020.100071.

[49] G. Yildiz, F. Ronsse, R. Venderbosch, R. van Duren, S.R.A. Kersten, W. Prins, Effect of biomass ash in catalytic fast pyrolysis of pine wood, Appl. Catal. B Environ. 168–169 (2015) 203–211, https://doi.org/10.1016/j.apcatb.2014.12.044.

[50] C.J. Gómez, E. Mészáros, E. Jakab, E. Velo, L. Puigjaner, Thermogravimetry/mass spectrometry study of woody residues and an herbaceous biomass crop using PCA techniques, J. Anal. Appl. Pyrolysis 80 (2007) 416–426, https://doi.org/10.1016/j.jaap.2007.05.003.

[51] S.V. Vassilev, D. Baxter, L.K. Andersen, C.G. Vassileva, T.J. Morgan, An overview of the organic and inorganic phase composition of biomass, Fuel 94 (2012) 1–33, https://doi.org/10.1016/j.fuel.2011.09.030.

[52] Y. Lu, Y. Wang, Q. Wang, J. Zhang, Y. Zhao, Y. Zhang, Investigation on the catalytic effect of AAEMs on the pyrolysis characteristics of Changji oil shale and its kinetics, Fuel 267 (2020), 117287, https://doi.org/10.1016/j.fuel.2020.117287.

[53] Q. Xiong, Y. Yang, F. Xu, Y. Pan, J. Zhang, K. Hong, et al., Overview of computational fluid dynamics simulation of reactor-scale biomass pyrolysis, ACS Sustain Chem. Eng. 5 (2017) 2783–2798, https://doi.org/10.1021/acssuschemeng.6b02634.

[54] D. Carpenter, T.L. Westover, S. Czernik, W. Jablonski, Biomass feedstocks for renewable fuel production: a review of the impacts of feedstock and pretreatment on the yield and product distribution of fast pyrolysis bio-oils and vapors, Green. Chem. 16 (2014) 384–406, https://doi.org/10.1039/C3GC41631C.

[55] S. Wang, X. Guo, K. Wang, Z. Luo, Influence of the interaction of components on the pyrolysis behavior of biomass, J. Anal. Appl. Pyrolysis 91 (2011) 183–189, https://doi.org/10.1016/j.jaap.2011.02.006.

[56] R.J. Evans, T.A. Milne, Molecular characterization of the pyrolysis of biomass, Energy Fuels 1 (1987) 123–137, https://doi.org/10.1021/ef00002a001.

[57] A. van Der Kaaden, J. Haverkamp, J.J. Boon, J.W. De Leeuw, Analytical pyrolysis of carbohydrates, J. Anal. Appl. Pyrolysis 5 (1983) 199–220, https://doi.org/10.1016/0165-2370(83)80028-X.

[58] Uncatalysed and potassium-catalysed pyrolysis of the cell-wall constituents of biomass and their model compounds. J Anal Appl Pyrolysis 2008;83:12–25. https://doi.org/10.1016/j.jaap.2008.05.007.

[59] A. Trendewicz, R. Evans, A. Dutta, R. Sykes, D. Carpenter, R. Braun, Evaluating the effect of potassium on cellulose pyrolysis reaction kinetics, Biomass-.-. Bioenergy 74 (2015) 15–25, https://doi.org/10.1016/j.biombioe.2015.01.001.

[60] H. Fan, J. Gu, Y. Wang, H. Yuan, Y. Chen, B. Luo, Effect of potassium on the pyrolysis of biomass components: pyrolysis behaviors, product distribution and kinetic characteristics, Waste Manag 121 (2021) 255–264, https://doi.org/10.1016/j.wasman.2020.12.023.

[61] C. Di Blasi, A. Galgano, C. Branca, Effects of potassium hydroxide impregnation on wood pyrolysis, Energy Fuels 23 (2009) 1045–1054, https://doi.org/10.1021/ef800827q.

[62] Y. Li, J. Wang, X. Chen, Z. Cheng, M. Xu, J. Yang, et al., Catalytic pyrolysis of xylan over alkali metal salts as revealed by synchrotron vacuum ultraviolet photoionization mass spectrometry, J. Anal. Appl. Pyrolysis 135 (2018) 94–100, https://doi.org/10.1016/j.jaap.2018.09.014.

[63] J. Klinger, E. Bar-Ziv, D. Shonnard, Unified kinetic model for torrefaction–pyrolysis, Fuel Process Technol. 138 (2015) 175–183, https://doi.org/10.1016/j.fuproc.2015.05.010.

[64] M. Carrier, M. Windt, B. Ziegler, J. Appelt, B. Saake, D. Meier, et al., Quantitative insights into the fast pyrolysis of extracted cellulose, hemicelluloses, and lignin, ChemSusChem 10 (2017) 3212–3224, https://doi.org/10.1002/cssc.201700984.

[65] D. Tamburini, J.J. Łucejko, E. Ribechini, M.P. Colombini, Snapshots of lignin oxidation and depolymerization in archaeological wood: an EGA-MS study, J. Mass Spectrom. 50 (2015) 1103–1113, https://doi.org/10.1002/jms.3631.

[66] E.R.E. van der Hage, M.M. Mulder, J.J. Boon, Structural characterization of lignin polymers by temperature-resolved in-source pyrolysis—mass spectrometry and Curie-point pyrolysis—gas chromatography/mass spectrometry, J. Anal. Appl. Pyrolysis 25 (1993) 149–183, https://doi.org/10.1016/0165-2370(93)80038-2.

[67] D. Kelly, A. Zerihun, D.P. Singh, C. Vitzthum von Eckstaedt, M. Gibberd, K. Grice, et al., Exposure of grapes to smoke of vegetation with varying lignin composition and accretion of lignin derived putative smoke taint compounds in wine, Food Chem. 135 (2012) 787–798, https://doi.org/10.1016/j.foodchem.2012.05.036.

[68] M.A. Scheijen, J.J. Boon, Micro-analytical investigations on lignin in enzyme-digested tobacco lamina and midrib using pyrolysis—mass spectrometry and Curie-point pyrolysis—gas chromatography / mass spectrometry, J. Anal. Appl. Pyrolysis 19 (1991) 153–173, https://doi.org/10.1016/0165-2370(91)80041-6.

[69] C.H. Vane, The molecular composition of lignin in spruce decayed by white-rot fungi (Phanerochaete chrysosporium and Trametes versicolor) using pyrolysis-GC–MS and thermochemolysis with tetramethylammonium hydroxide, Int Biodeterior. Biodegrad 51 (2003) 67–75, https://doi.org/10.1016/S0964-8305(02)00089-6.

[70] M. Mattonai, A. Watanabe, A. Shiono, E. Ribechini, Degradation of wood by UV light: a study by EGA-MS and Py-GC/MS with on line irradiation system, J. Anal. Appl. Pyrolysis 139 (2019) 224–232, https://doi.org/10.1016/j.jaap.2019.02.009.

[71] L. Burhenne, J. Messmer, T. Aicher, M.-P. Laborie, The effect of the biomass components lignin, cellulose and hemicellulose on TGA and fixed bed pyrolysis, J. Anal. Appl. Pyrolysis 101 (2013) 177–184, https://doi.org/10.1016/j.jaap.2013.01.012.

[72] H. Haykiri-Acma, S. Yaman, S. Kucukbayrak, Effect of heating rate on the pyrolysis yields of rapeseed, Renew. Energy 31 (2006) 803–810, https://doi.org/10.1016/j.renene.2005.03.013.

[73] Hernan Almuina-Villar, Peter Sommersacher, Stefan Retschitzegger, Andres Anca-Couce, Alba Dieguez-Alonso, Combined influence of inorganics and transport limitations on the pyrolytic behaviour of woody biomass, Chem. Eng. Trans. 80 (2020) 73–78, https://doi.org/10.3303/CET2080013.

[74] S. Sobek, S. Werle, Solar pyrolysis of waste biomass: Part 2 kinetic modeling and methodology of the determination of the kinetic parameters for solar pyrolysis of sewage sludge, Renew. Energy 153 (2020) 962–974, https://doi.org/10.1016/j.renene.2020.02.061.

[75] J. Bonilla, R.P. Salazar, M. Mayorga, Kinetic triplet of Colombian sawmill wastes using thermogravimetric analysis, Heliyon 5 (2019), e02723, https://doi.org/10.1016/j.heliyon.2019.e02723.

[76] E. Biagini, F. Lippi, L. Tognotti, Characterization of a lab-scale platinum filament pyrolyzer for studying the fast devolatilization of solid fuels, Fuel 85 (2006) 2408–2418, https://doi.org/10.1016/j.fuel.2006.06.002.

[77] J.E. White, W.J. Catallo, B.L. Legendre, Biomass pyrolysis kinetics: a comparative critical review with relevant agricultural residue case studies, J. Anal. Appl. Pyrolysis 91 (2011) 1–33, https://doi.org/10.1016/j.jaap.2011.01.004.

[78] C. Zhu, C. Krumm, G.G. Facas, M. Neurock, P.J. Dauenhauer, Energetics of cellulose and cyclodextrin glycosidic bond cleavage, React. Chem. Eng. 2 (2017) 201–214, https://doi.org/10.1039/C6RE00176A.
[79] M.G. Grønli, G. Várhegyi, C. Di Blasi, Thermogravimetric analysis and devolatilization kinetics of wood, Ind. Eng. Chem. Res 41 (2002) 4201–4208, https://doi.org/10.1021/ie0201157.
[80] A. Anca-Couce, Reaction mechanisms and multi-scale modelling of lignocellulosic biomass pyrolysis, Prog. Energy Combust. Sci. 53 (2016) 41–79, https://doi.org/10.1016/j.pecs.2015.10.002.
[81] J. Zhang, T. Chen, J. Wu, J. Wu, Multi-Gaussian-DAEM-reaction model for thermal decompositions of cellulose, hemicellulose and lignin: Comparison of N2 and CO_2 atmosphere, Bioresour. Technol. 166 (2014) 87–95, https://doi.org/10.1016/j.biortech.2014.05.030.
[82] T. Chen, L. Li, R. Zhao, J. Wu, Pyrolysis kinetic analysis of the three pseudocomponents of biomass–cellulose, hemicellulose and lignin, J. Therm. Anal. Calor. 128 (2017) 1825–1832, https://doi.org/10.1007/s10973-016-6040-3.
[83] J. Zhang, T. Chen, J. Wu, J. Wu, A novel Gaussian-DAEM-reaction model for the pyrolysis of cellulose, hemicellulose and lignin, RSC Adv. 4 (2014) 17513–17520, https://doi.org/10.1039/C4RA01445F.
[84] P. Murugan, N. Mahinpey, K.E. Johnson, M. Wilson, Kinetics of the pyrolysis of lignin using thermogravimetric and differential scanning calorimetry methods, Energy Fuels 22 (2008) 2720–2724, https://doi.org/10.1021/ef700730u.
[85] E. Avni, R.W. Coughlin, Kinetic analysis of lignin pyrolysis using non-isothermal TGA data, Thermochim. Acta 90 (1985) 157–167, https://doi.org/10.1016/0040-6031(85)87093-3.
[86] T. Mani, P. Murugan, N. Mahinpey, Determination of distributed activation energy model kinetic parameters using simulated annealing optimization method for nonisothermal pyrolysis of lignin, Ind. Eng. Chem. Res 48 (2009) 1464–1467, https://doi.org/10.1021/ie8013605.
[87] C. Di Blasi, C. Branca, Kinetics of primary product formation from wood pyrolysis, Ind. Eng. Chem. Res 40 (2001) 5547–5556, https://doi.org/10.1021/ie000997e.
[88] B.M. Wagenaar, W. Prins, W.P.M. van Swaaij, Flash pyrolysis kinetics of pine wood, Fuel Process Technol. 36 (1993) 291–298, https://doi.org/10.1016/0378-3820(93)90039-7.
[89] J. Lédé, Cellulose pyrolysis kinetics: an historical review on the existence and role of intermediate active cellulose, J. Anal. Appl. Pyrolysis 94 (2012) 17–32, https://doi.org/10.1016/j.jaap.2011.12.019.
[90] M. Bhattacharyya, K.P. Shadangi, P. Mahanta, K. Mohanty, Co-pyrolysis of coal-biomass: study on reaction kinetics and thermodynamics, Biofuels Bioprod. Bioref. 16 (2022) 725–742, https://doi.org/10.1002/bbb.2333.
[91] M.J. Molina, L.T. Molina, C.A. Smith, The rate of the reaction of OH with HCl, Int J. Chem. Kinet. 16 (1984) 1151–1160, https://doi.org/10.1002/kin.550160910.
[92] S.V. Vyazovkin, V.I. Goryachko, A.I. Lesnikovich, An approach to the solution of the inverse kinetic problem in the case of complex processes. Part III. Parallel independent reactions, Thermochim. Acta 197 (1992) 41–51, https://doi.org/10.1016/0040-6031(92)87037-B.
[93] O.S. Al-Ayed, M.W. Amer, M. Matouq, Variable activation energy principle to model oil shale pyrolysis kinetics, Oil Shale 34 (2017) 181–194, https://doi.org/10.3176/oil.2017.2.07.
[94] R.R. Nair, M.M. Mondal, S.V. Srinivasan, D. Weichgrebe, Biochar synthesis from mineral- and ash-rich waste biomass, part 1: investigation of thermal decomposition mechanism during slow pyrolysis, Materials 15 (2022) 4130, https://doi.org/10.3390/ma15124130.